University of Liège
Faculty of Applied Sciences - Second Master's Degree in Civil Engineering

Wind pressure field reconstruction from incomplete measurements

Master's Thesis

submitted in partial fulfillment of the requirements for the degree of

Master in Civil Engineering

Conducted by Andy Fossion

Supervisor : Professor V. Denoël

Jury composition:

Prof. J-P. Jaspart, president (ULg)
Prof. V. Denoël, thesis supervisor (ULg)
Prof. L. Carassale, co-supervisor (UniGe)
Prof. V. de Ville de Goyet, member (ULg)
Dr. T. Andrianne, member (ULg)

Academic year 2014-2015

Tout obstacle renforce la détermination. Celui qui s'est fixé un but n'en change pas.
Leonardo da Vinci

Wind pressure field reconstruction from incomplete measurements by Andy Fossion, Second Master's Degree in Civil Engineering, University of Liège, academic year 2014-2015.

The purpose of this master's thesis is to develop a method to reconstruct missing data from multiple setup measurements in wind tunnel. It is obtained using the singular value decomposition on the measured values. This mathematical tool extracts the main direction of a rectangular matrix. With appropriate experimental setups, these directions tend to be similar to the ones from the complete matrix with all measurements made synchronously. This method is numerically applicable thanks to the background/resonant decomposition, which reduces the amount of reconstruction steps needed. The method developed is applied on a high-rise building in order to quantify its accuracy. Several multiple setup schemes are presented and compared to the reference results.

Keywords: wind; wind tunnel; buildings; multiple setup measurements; stochastic; background response; resonant response; singular value decomposition; reconstruction; modal correlation.

Reconstruction de champ de pression de vent à partir de données manquantes par Andy Fossion, Deuxième année de Master Ingénieur civil des constructions, Université de Liège, année académique 2014-2015.

L'objectif de cette thèse de master est de développer une méthode de reconstruction de données manquantes provenant d'essais à configurations multiples réalisés en soufflerie. La méthode est obtenue en appliquant la décomposition en valeurs singulières sur les données mesurées. Cet outil mathématique permet d'extraire les directions principales d'une matrice rectangulaire. En utilisant des configurations expérimentales appropriées, ces directions tendent à être similaires à celles de la matrice complète obtenue avec les mesures synchrones. Cette méthode est applicable numériquement grâce à la décomposition background/résonant qui permet de réduire le nombre nécessaire de reconstructions. La méthode développée est appliquée à un building de grande hauteur dans le but de quantifier sa précision. Plusieurs schéma de configurations expérimentales multiples sont présentés et comparés aux résultats de référence.

Mots-clés: vent; soufflerie; buildings; mesures à configurations multiples; stochastique; réponse background; réponse résonante; décomposition en valeurs singulières; reconstruction; corrélation modale.

Acknowledgement

I would like to express my sincere gratitude to my supervisor Prof. Denoël for the continuous guidance of my master's thesis, his enthusiasm for this work and his clever advices.

My sincere thanks also goes to Prof. Carassale for the warm welcome in Genoa and his precious help during my stay there.

I would also like to say a special thanks to my parents for their love and the support in everything I undertook throughout my life.

I'm grateful to my friends who allows me to have fun and relax between the hard working sessions.

And eventually, I would like to thanks Adeline, my partner, for her support, her love and for everything since 6 years.

Contents

Part I

Context and motivations

Chapter 1

Introduction

Nowadays, buildings and civil works are getting taller, bigger and more sophisticated. Beyond the increasing complexity of these structures, the consequences of a failure would have a dramatic impact from a human and an economical point of view. This general evolution leads civil engineers to develop new designing methods that consider dynamic phenomena and estimate both the displacement and the internal forces due to these time and space fluctuating loads.

Beside seismic solicitations, one of the main cause for **dynamic phenomena** is the **wind**. The randomness and the dynamic nature of the wind make it difficult to approach with simple methods. Different solutions exist to find the resulting wind pressure field on a structure such as CFD analysis, wind tunnel experiment on a scaled model or on site measurements. All of them have advantages and drawbacks. That is the reason why they are usually done in a complementary manner.

This work focuses on the second one, **wind tunnel experiment**. This approach consists in using a scaled model of the structure to design, which is placed in a small scale atmospheric boundary layer. Different layers could be used such as logarithmic or power law in order to take into account the roughness of the ground.

The objective of wind tunnel experiments is to measure the evolution over time of some physical quantities. In the case of a rigid model, the main information is the pressure on the structure induced by the wind.

To capture this information a certain amount of pressure sensors is needed. Considering that the amount of sensors at our disposal is not limited, the best solution would be to cover uniformly and densely enough all the structure with them. In that way, we would have not only the information about the evolution of the pressure at each point but also the correlation between all of them since they are measured synchronously.

Unfortunately, this situation is utopian and most of the time, experimental engineers have a limited amount of sensors. It means that it is not possible to cover the whole structure with enough density of sensors. In other words, a lot of information for the design is not recorded.

The solution to face this issue is to use **multiple setup measurements**. The main idea behind it is to set some reference sensors at strategic places on the structure and to

move the other ones across the structure. After the test, the evolution of the pressure over time of each sensors and partial information on the relation between them is known.

To illustrate the multiple setup measurements principle, we can consider a wind tunnel experiment where the model would be a small rectangular plate with a perpendicular wind flow. Two different situations are considered. In the first situation, three sensors are available. It is enough to cover the plate densely enough with one sensor at the top, at the middle and at the bottom. Then, in the second situation, only two sensors are available, which is not enough to cover the whole plate and to capture all the information needed to design this plate. A solution would be to fix a reference sensor in the middle of the plate and to move the other one in the upper and the lower part so that two experimental setups are conducted.

Eventually, the measurements can be done so that we have in the first situation the evolution of the pressure over the same time series.

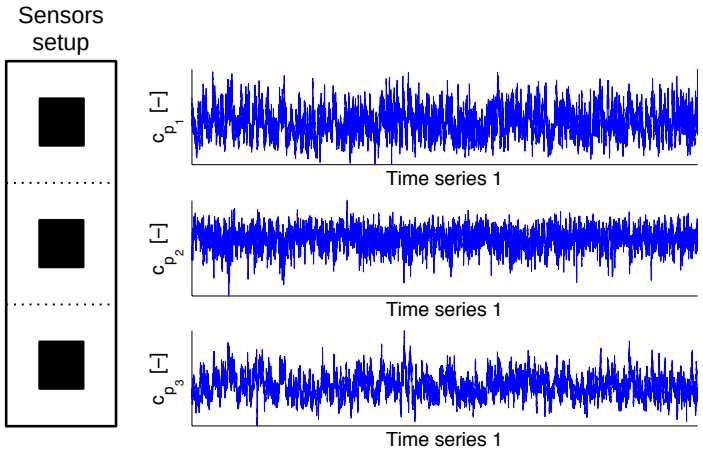

Figure I.1.1: Synchronous measurements.

In the second situation, we also have the evolution of the pressure but this time over two different time series since they are not measured synchronously.

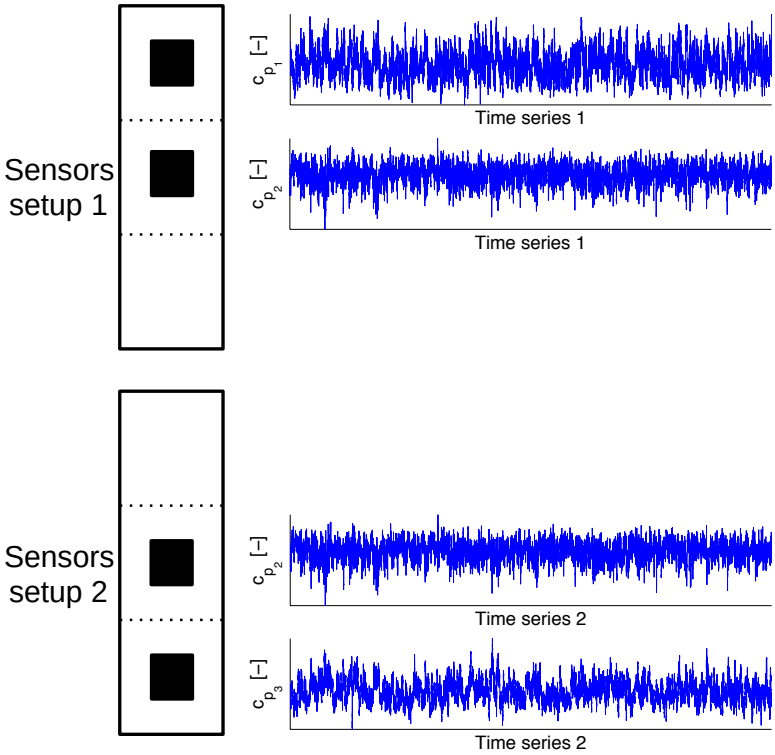

Figure I.1.2: Multiple setup measurements.

For each sensor, the mean, the standard deviation and the variance can be calculated for the evolution of pressure. This information should be similar in both situations. Next to these properties, it is also possible to compute their statistical relation, such as the **covariance or the correlation coefficient**. One property of these values is that the samples from which they are calculated must have the same time series. This point highlights the main difference between the two situations presented, the covariance of sensors that are not measured synchronously can not be calculated.

It means that after the two experiments, we have at our disposal two different covariance matrices :

$$C_{p_{Sync}} = \begin{pmatrix} \sigma_1^2 & \sigma_{12}^2 & \sigma_{13}^2 \\ \sigma_{12}^2 & \sigma_2^2 & \sigma_{23}^2 \\ \sigma_{13}^2 & \sigma_{23}^2 & \sigma_3^2 \end{pmatrix} \tag{I.1.1}$$

$$C_{p_{Mult}} = \begin{pmatrix} \sigma_1^2 & \sigma_{12}^2 & \bullet \\ \sigma_{12}^2 & \sigma_2^2 & \sigma_{23}^2 \\ \bullet & \sigma_{23}^2 & \sigma_3^2 \end{pmatrix}. \tag{I.1.2}$$

The first one, from the synchronous measurements, which is full and the second one from multiple setups, which is incomplete. Here is the starting point of this thesis. The main goal is to find a way to guess the covariance between sensors 1 and 3. In that purpose, it is assume that it exists a relation between the two covariances known, σ_{12}^2 and

σ^2_{23} and the covariance searched,σ^2_{13}. In the limit case of a perfect correlation between 1 and 2 and between 2 and 3, there is no other choice that sensors 1 and 3 are also fully correlated.

This step is called the **reconstruction** of the missing information. In this work, we develop a non-parametric method that could be applied in different situations. Indeed, the usage of this approach is wide and appears in all the domain where multiple setup measurements are done such as in aeronautic or in mechanics. It means that the perspectives behind this thesis may be large.

To focus on the field of civil engineering, the chosen model to develop this method is a prism building described in the following chapter. Firstly, we try to verify the reliability of the chosen model and apply a standard analysis in order to get reference results. Then, the analysis of the method is made and compared to the reference analysis to have an estimation of its accuracy.

It is worth noticing that beyond the fundamental research interest, this work could also have an important **economical impact** for companies that want to conduct wind tunnel experiments on their own structural projects. Indeed, the main goal of this thesis is to find a way to work accurately with a limited number of sensors but it could be turned into reducing intentionally the number of sensors in order to reduce the price of the experiment.

Two factors mainly govern the final cost of a wind tunnel campaign on a model : the material used and the labour. In other words, either the number of the pressure taps or the number of setups can be reduced. Of course these two variables are linked and it is not possible to reduce both of them infinitely, keeping the accuracy constant.

To find a tradeoff, the relation between the two variables has to be found. It means the number of setups needed for a certain amount of pressure taps to keep enough accuracy. Then the cost need to be expressed as a function of the number of pressure taps and as a function of the number of setups.

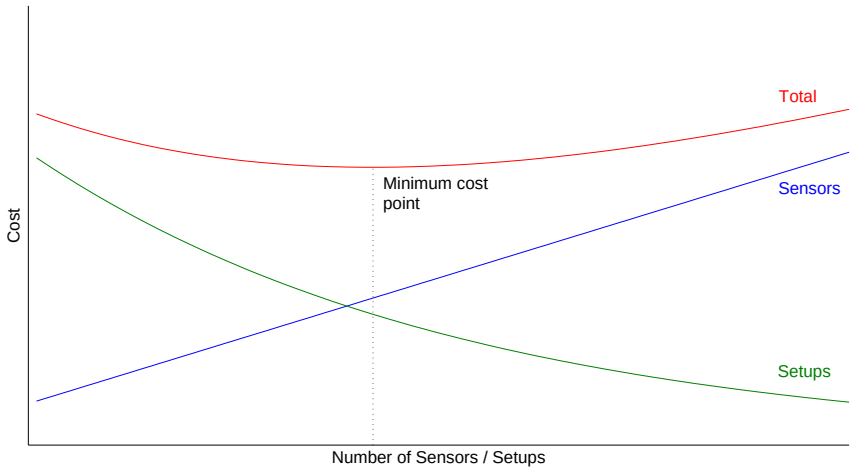

Figure I.1.3: Minimisation of the cost as a function of the number of sensors and setups.

For the first one, the price of one sensor is fixed. It means that the cost increases linearly with the number of pressure taps. For the second one, an exponential curve is used. The marginal cost decreases with the number of setups. Indeed, the increasing cost from 1 to 2 setups is higher than from 10 to 11 setups.

Eventually, the total cost is calculated for each pair [N^{br} setups,N^{br} sensors] and a minimum is found. This minimum is the economical optimum.

The purpose of this thesis is not to define the perfect economical multiple setup but it is worth noticing that the interest of this method can also be economical. For that reason, we did not plot the graph above with specific values on the axis to keep the concept general.

Chapter 2

Considered case study

In 1997, Professors Kikuchi, Tamura, Ueda and Hibi from Japan conducted different wind-tunnel experiments to investigate the properties of the wind pressure on tall building using the Proper Orthogonal Decomposition (POD) technique as a post-processing tool. This method is used to capture the most energetic terms in a general process [1]. In wind engineering, it would allow us to express the whole pressure field with only a few dominant modes.

In other words, the purpose of the analysis is to find a function that will correlate in the best way all the elements of the fluctuating wind pressure field. The mathematical expression of this problem is the maximisation of the projection from the fluctuating pressure field $p(x, y, t)$ into the deterministic function $\Phi(x, y)$:

$$\int\int p(x, y, t)\Phi(x, y)dxdy \text{ is maximum.} \tag{I.2.1}$$

Using a mean square method to solve this problem and considering the fluctuating wind pressure as discretized, it can be written in the matrix form

$$\mathbf{R_p\Phi} = \lambda\mathbf{\Phi} \tag{I.2.2}$$

where R_p is a spatial correlation matrix of the fluctuating wind pressure. Symbols Φ and λ denote an eigenvector and an eigenvalue of the spatial correlation matrix R_p, respectively [2].

Eventually, it can be shown that with only 65 modes, 90% of the original pressure field can be obtained [3]. This observation highlights that the main part of the information given by the 500 taps is redundant. Indeed, we do not need that much degrees of freedom (pressure taps) to extract all the information contained in the wind. Reducing the number of pressure taps takes on its full meaning.

2.1 Experimental Setup

These experiments were conducted in boundary layer wind tunnel with a cross section of 2.6 x 2.4 m. An approaching wind with a length scale of $\frac{1}{400}$ for suburban terrain with a

power-law was used. This law is defined as:

$$U(z) = U_{ref}(\frac{z}{z_{ref}})^{\alpha} \tag{I.2.3}$$

where U_{ref} is the reference velocity of the wind, z_{ref} the height at which the boundary condition has no more influence and α a parameter of the law equal in our case to $\frac{1}{6}$.

The tall building model used is a rectangular prism with the following dimensions, 0.5 x 0.1 x 0.1 m. On the four faces were placed 125 pressure taps uniformly distributed between 5 columns and 25 rows.

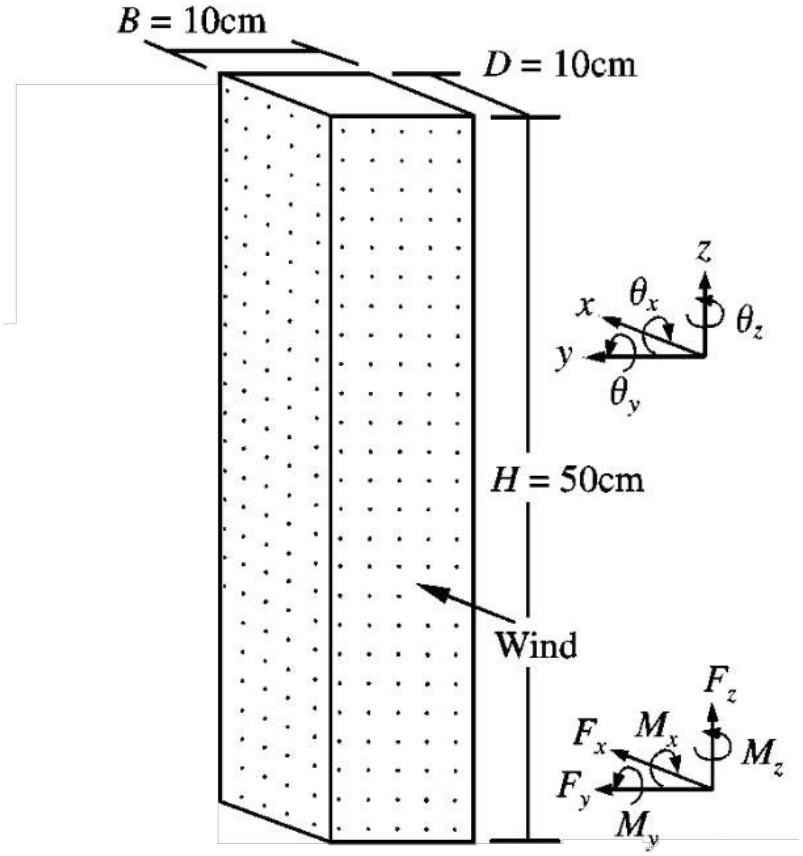

Figure I.2.1: Reference model.

All the pressures from the four faces were measured in a synchronous way. The sampling interval of the fluctuating wind pressure was 1 ms and the 32768 samples were obtained continuously [2].

Different angles of attack were used, from 0° to 45°. We will only focus on three of them: 0°, 15° and 45°. In order to simplify the comprehension of this paper, we named the faces as shown in the figure below.

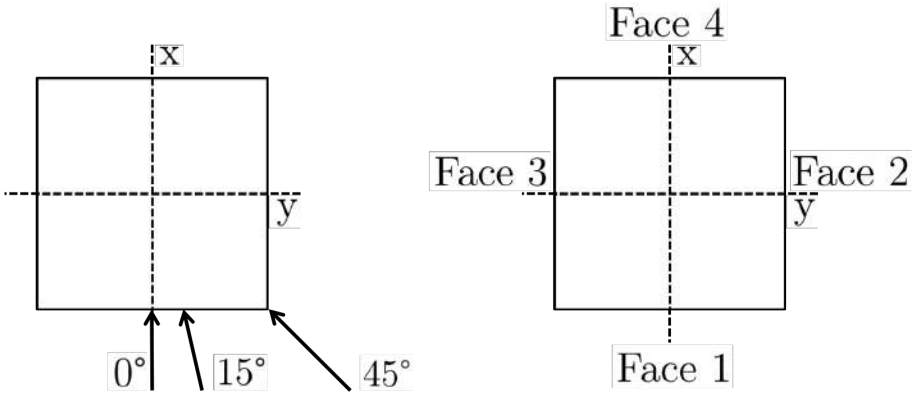

Figure I.2.2: Flow angles and faces names

2.2 Results

In order to have an idea of the resultant pressure field on the structure, it is worth looking at its mean and its variance. These two quantities are represented by contour line on each face.

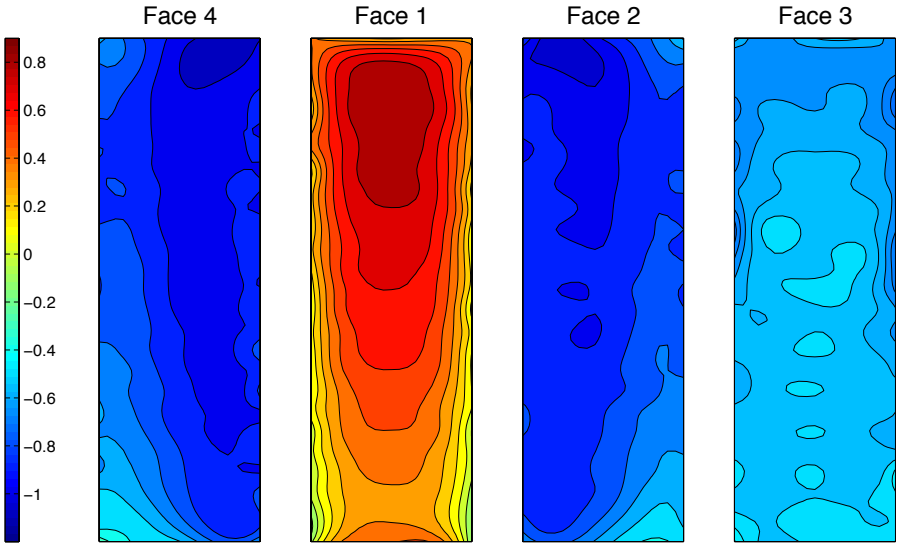

Figure I.2.3: Mean pressure on the four faces for an angle of attack of 0°.

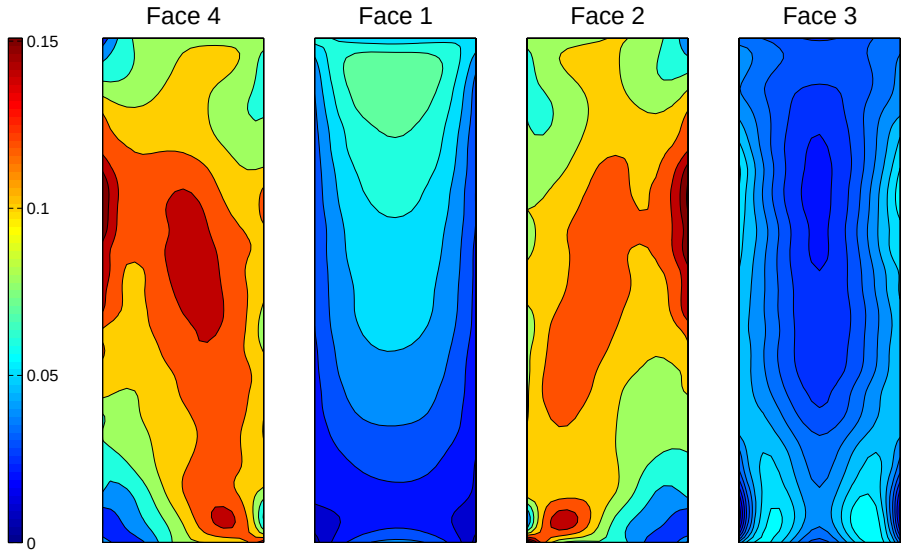

Figure I.2.4: Variance of the pressure on the four faces for an angle of attack of 0°.

For an angle of attack of 0°, the wind pressure wind can be considered as symmetrical. The mean pressure is positive on the first face and negative on the three others and the magnitude is more important on the two lateral faces. Concerning the variance, it is small on the two faces perpendicular to the wind flow and is more important on the two laterals faces. This observations is explained by the vortex shedding phenomena that will be discussed further afterwards.

The figures related to the other angles of attack are presented in the *Appendix A*.

2.3 Motivations

The motivation behind this choice is twofold. Firstly, the density of sensors used by the experimenters is high. It means that we have of lot of information at our disposal. It also means that when we will try to reduce manually the number of pressure taps, we will have the chance to try different configurations.

Secondly, we want to develop a method that is as general as possible. Indeed, we want to focus on the applied method and not on the specific results induced by the geometrical particularities of the building. Moreover, the measurements made by *Kikuchi & al.* has already been treated and studied many times since the experiments were conducted. We can thus rely on them and focus again only on the process developed.

Despite this will of using a simple model to develop a general method, a lot of building are directly concerned. Indeed, besides the fight of uniqueness between the architects, a lot of new buildings are still parallelepipedic as shown in figure I.2.5.

Figure I.2.5: Goldin Finance 117 in Tianjin (2015) on the left and the World Trade Center 3 in Beijing on the right (2008)

Part II

Theoretical Aspects

This part summarises the main theoretical aspects and introduces the notations that are used in the rest of the manuscript. All the information presented are inspired from [4], [5] and [6].

Chapter 1

The Finite Element Method

A common way to analyse structures is to use the finite element method. The real structure is modeled by a certain amount of elements connected to each others at nodes. Only the displacements of these nodes will be studied. Each node has six degrees of freedom, three translations and three rotations. When studying a tall building, it is usual to neglect the deformation along the axis of the element. Thus, five degrees of freedom for each node are considered.

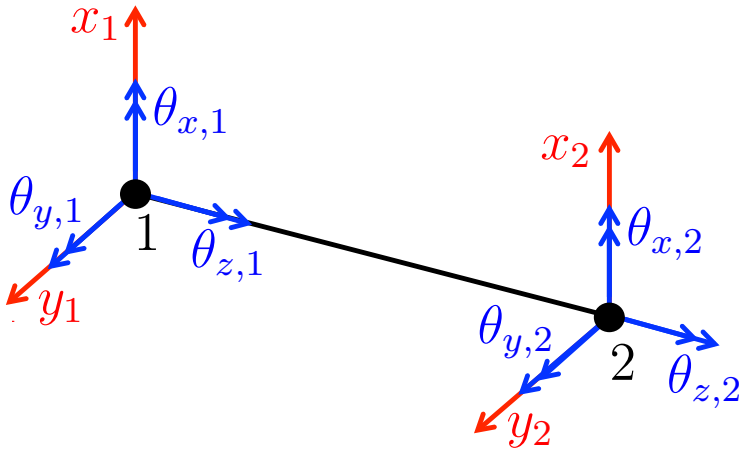

Figure II.1.1: Degrees of freedom of an element.

The elements have structural properties such as mass, stiffness and damping that need to be defined. Once it is done, the properties of these elements are combined in order to get global matrices, which are related to the complete structure.

1.1 Resolution of the system

The general equation of the FEM is given by:

$$\mathbf{K}_{global}\mathbf{x} = \mathbf{F}_{global} \tag{II.1.1}$$

which is the relation between the forces applied on the system, $\mathbf{F}_{global}$, and its displacements, $\mathbf{x}$. These two are linked by a stiffness matrix $\mathbf{K}_{global}$. If we are looking at a dynamic system, a mass and a damping matrice should also be considered in order to find the displacements.

1.1.1 Stiffness and mass matrices

The local stiffness matrix of an element is defined in the following way:

$$\mathbf{K}_{element} = EI \begin{pmatrix} \frac{12}{L^3} & 0 & 0 & 0 & \frac{6}{L^2} & \frac{-12}{L^3} & 0 & 0 & 0 & \frac{6}{L^2} \\ 0 & \frac{12}{L^3} & 0 & \frac{-6}{L^2} & 0 & 0 & \frac{-12}{L^3} & 0 & \frac{-6}{L^2} & 0 \\ 0 & 0 & \frac{GJ}{EIL} & 0 & 0 & 0 & 0 & \frac{-GJ}{EIL} & 0 & 0 \\ 0 & \frac{-6}{L^2} & 0 & \frac{4}{L} & 0 & 0 & \frac{6}{L^2} & 0 & \frac{2}{L} & 0 \\ \frac{6}{L^2} & 0 & 0 & 0 & \frac{4}{L} & \frac{-6}{L^2} & 0 & 0 & 0 & \frac{2}{L} \\ \frac{-12}{L^3} & 0 & 0 & 0 & \frac{-6}{L^2} & \frac{12}{L^3} & 0 & 0 & 0 & \frac{-6}{L^2} \\ 0 & \frac{-12}{L^3} & 0 & \frac{6}{L^2} & 0 & 0 & \frac{12}{L^3} & 0 & \frac{6}{L^3} & 0 \\ 0 & 0 & \frac{-GJ}{EIL} & 0 & 0 & 0 & 0 & \frac{GJ}{EIL} & 0 & 0 \\ 0 & \frac{-6}{L^2} & 0 & \frac{2}{L} & 0 & 0 & \frac{6}{L^2} & 0 & \frac{4}{L} & 0 \\ \frac{6}{L^2} & 0 & 0 & 0 & \frac{2}{L} & \frac{-6}{L^2} & 0 & 0 & 0 & \frac{4}{L} \end{pmatrix} = \begin{pmatrix} k_{1,1}^{element} & k_{1,2}^{element} \\ k_{2,1}^{element} & k_{2,2}^{element} \end{pmatrix}.$$

Note that the dofs are ordered in the following way: $(x_1, y_1, \theta_{z,1}, \theta_{x,1}, \theta_{y,1}, x_2, y_2, \theta_{z,2}, \theta_{x,2}, \theta_{y,2})$.

For the mass, the Euler-Bernoulli matrix given as follow will be used:

$$\mathbf{M}_{element} = \frac{\mu L}{420} \begin{pmatrix} 156 & 0 & 0 & 0 & 22L & 54 & 0 & 0 & 0 & -13L \\ 0 & 156 & 0 & -22L & 0 & 0 & 54 & 0 & 13L & 0 \\ 0 & 0 & \frac{140It}{A} & 0 & 0 & 0 & 0 & \frac{70It}{A} & 0 & 0 \\ 0 & -22L & 0 & 4L^2 & 0 & 0 & -13L & 0 & -3L^2 & 0 \\ 22L & 0 & 0 & 0 & 4L^2 & 13L & 0 & 0 & 0 & -3L^2 \\ 54 & 0 & 0 & 0 & 13L & 156 & 0 & 0 & 0 & -22L \\ 0 & 54 & 0 & -13L & 0 & 0 & 156 & 0 & 22L & 0 \\ 0 & 0 & \frac{70It}{A} & 0 & 0 & 0 & 0 & \frac{140It}{A} & 0 & 0 \\ 0 & 13L & 0 & -3L^2 & 0 & 0 & 22L & 0 & 4L^2 & 0 \\ -13L & 0 & 0 & 0 & -3L^2 & -22L & 0 & 0 & 0 & 4L^2 \end{pmatrix}.$$

These two matrices are related to one element. The damping matrix is defined afterwards using the *Rayleigh* approximation and the modal decomposition.

1.1.2 Work-equivalent applied forces

The next step is to define the work-equivalent applied forces matrix. The main idea is to integrate the load on the element in order to replace it by punctual forces applied on the adjacent nodes. To illustrate this, an element uniformly loaded along one axis only is considered.

This process is applicable along the x and y axis. Concerning the work equivalent torsion, the process is similar and the assumption of a constant torsion along the element is done. The integrated torsion is spread between the two adjacent nodes.

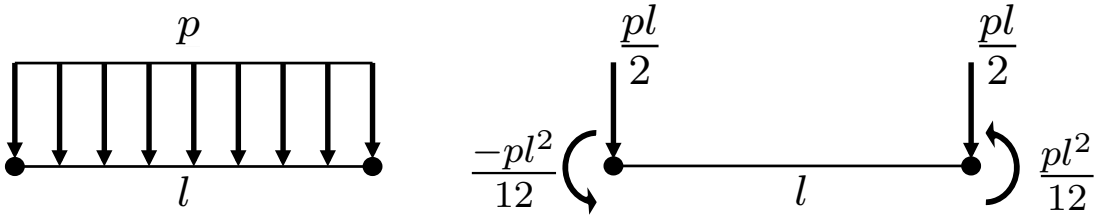

Figure II.1.2: Work-equivalent applied forces

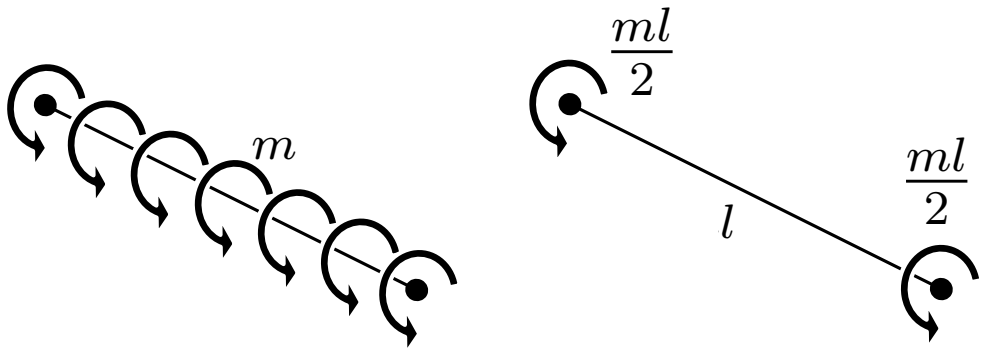

Figure II.1.3: Work-equivalent applied torsions

Again, the values are defined for an element. It is then necessary to build the complete work equivalent force matrix by taking into account that most of the nodes are loaded by two elements.

In a practice, an influence matrix will be defined in order to get the nodal forces from the pressure at each point of the structure:

$$\mathbf{F}(t) = \mathbf{A}\mathbf{p}(t) \tag{II.1.2}$$

where $\mathbf{A}$ is called the influence matrix, which is related to the position of the pressure taps.

Chapter 2

Structural analysis

The general purpose of structural analysis is to determine both the displacements and the internal forces of a structure in order to design it. When the structural response is dynamic, inertial and damping terms must be considered in addition to of the stiffness term. Eventually, the complete equation of movement is written,

$$\mathbf{M}\ddot{\mathbf{x}}(t) + \mathbf{C}\dot{\mathbf{x}}(t) + \mathbf{K}\mathbf{x}(t) = \mathbf{f}(t). \tag{II.2.1}$$

where $\mathbf{M}$ is the mass matrix, $\mathbf{C}$ the damping matrix and $\mathbf{K}$ the stiffness matrix. The load $\mathbf{f}(t)$ and the displacement $\mathbf{x}(t)$ are given as an evolution over time of all the degrees of freedom.

2.1 Modal decomposition

Instead of the solving the system with the nodal displacement as unknown, it is possible to express the displacement as a combination of vibration modes. These modes are defined by a shape and an amplitude. The unknowns are no longer the values of $\mathbf{x}(t)$ but the modal amplitude $\mathbf{q}(t)$ so that:

$$\mathbf{x}(t) = \boldsymbol{\phi}\mathbf{q}(t) = \Sigma\phi_i q_i \tag{II.2.2}$$

where ϕ_i represents the shape of the i^{th} natural mode normalised as maximum unitary and $\mathbf{q}_i$ its magnitude. The matrices $\mathbf{M}$,$\mathbf{C}$ and $\mathbf{K}$ must be projected in the modal basis to get the generalised mass, stiffness and viscosity matrices related to the modal basis:

$$\mathbf{M}^* = \boldsymbol{\phi}^T\mathbf{M}\boldsymbol{\phi} \tag{II.2.3}$$
$$\mathbf{K}^* = \boldsymbol{\phi}^T\mathbf{K}\boldsymbol{\phi} \tag{II.2.4}$$
$$\mathbf{C}^* = \alpha\mathbf{M}^* + \beta\mathbf{K}^*. \tag{II.2.5}$$

These three matrices are diagonal. The generalised forces must also be calculated:

$$\mathbf{f}^*(t) = \phi^T\mathbf{f}(t). \tag{II.2.6}$$

The equation of movement (II.2.1) can be rewritten in the modal basis:

$$\mathbf{M}^*\ddot{\mathbf{q}}(t) + \mathbf{C}^*\dot{\mathbf{q}}(t) + \mathbf{K}^*\mathbf{q}(t) = \mathbf{f}^*(t). \tag{II.2.7}$$

The modal approach appears to be useful for different reasons. Firstly, all the vibration modes should not be used in the analysis. Indeed, the response takes place in only a few dominant modes. Then, it allows to reduce the number of unknowns and to solve the system only for these specifics modes. We will discuss further which modes should be considered to keep on getting an accurate approximation of the response.

Secondly, the system is made of independent equations. Indeed, the structural matrices are diagonal in the modal basis. In other words, it allows to solve each equation of the system in the same manner as a singular degree of freedom structure.

Note that the modal basis is well adapted when the response is dynamic. On the other hand, some discrepancy might appear when the response is quasi-static due to the modal truncation.

2.1.1 Damping matrix

The *Rayleigh* approximation is used to determine the damping matrix. It consists of a linear combination of the matrices $\mathbf{M}$ and $\mathbf{K}$.

The parameters used in this linear interpolation ω_1, ω_3 are the two first natural pulsations both in the x et y direction because of the symmetry. They are determined by calculating $det(\mathbf{K} - \mathbf{M}\omega^2) = 0$ and finding the N roots of the characteristic polynomial. The values ω_i are positive, because $\mathbf{M}$ and $\mathbf{K}$ are positive definite. They are ordered in such a way: $0 < \omega_1^2 \leq \omega_2^2 \leq ... \leq \omega_N^2$.

The damping matrix can be written,

$$\mathbf{C} = \alpha\mathbf{M} + \beta\mathbf{K} \tag{II.2.8}$$

where the two coefficients α and β are found with the following equations,

$$\alpha = \frac{2\omega_1\xi}{\omega_1 + \omega_3} \tag{II.2.9}$$

$$\beta = \frac{2\omega_1\omega_3\xi}{\omega_1^2 - \omega_3^2}\left(\frac{1}{\omega_1} - \frac{1}{\omega_3}\right). \tag{II.2.10}$$

Note that the damping ratio ξ is chosen constant between the two first vibration modes in each direction.

2.2 Deterministic approach

A deterministic model is defined as "a mathematical representation of a system in which relationships are fixed (i.e. taking no account of probability), so that any given input invariably yields the same result" [7].

In other words, all the results obtained in terms of displacements or internal forces are fully determined by the system parameters and the initial conditions. This approach is in opposition with the stochastic approach, which introduces the notion of probability.

To solve our problem in a deterministic way, we have two options. The first one is to express the displacement as a function of time. The second one is to apply the Fourier transform to our sample in order to get the results as a function of the frequency. Both options are briefly discussed and are applied to the model in order to verify the consistency of the results.

2.2.1 Time domain analysis

The time domain analysis consists in solving the fundamental equation as function of time. The equations of the modal system are independent. Using a simple linear solver, the fundamental equation can be written in the following way:

$$\dot{\mathbf{z}}(t) = \mathbf{A}\mathbf{z}(t) + \mathbf{B}\mathbf{u}(t) \tag{II.2.11}$$

Since the analysis is done in the modal basis, $\mathbf{q}(t)$ is the modal displacements vector, $\mathbf{z}(t) = \begin{bmatrix}\mathbf{q}(t)\\ \dot{\mathbf{q}}(t)\end{bmatrix}$ and $\mathbf{u}(t)$ is the modal forces vector. The two matrices $\mathbf{A}$ and $\mathbf{B}$ are defined as:

$$\mathbf{A}_{[2N\times 2N]} = \begin{bmatrix}\mathbf{O}_N & \mathbf{I}_N\\ -\mathbf{M}^{*-1}\mathbf{K}^* & -\mathbf{M}^{*-1}\mathbf{C}^*\end{bmatrix} \tag{II.2.12}$$

$$\mathbf{B}_{[2N\times N]} = \begin{bmatrix}\mathbf{O}_N\\ \mathbf{M}^{*-1}\end{bmatrix} \tag{II.2.13}$$

where N is equal to the number of modes considered in the analysis, $\mathbf{O}_N$ is a N $\times$ N matrix full of zero and $\mathbf{I}_N$ is a N $\times$ N identity matrix.

In order to limit the unsteady response at the beginning, the quasi-static displacement is used as initial condition. It is defined as:

$$\mathbf{q}_{qs}(t) = \mathbf{K}^{*-1}\mathbf{f}^*(t). \tag{II.2.14}$$

The initial velocity is supposed to be null.

2.2.2 Frequency domain analysis

The second possibility to solve the fundamental equation in a deterministic way is to use the frequency domain analysis. This solution is really useful when working in the full basis because it allows us to replace the convolution product by a simple multiplication.

The Fourier transform is applied directly on the fundamental equation and the

resulting system is integrated by parts.

$$\int_{-\infty}^{+\infty}(\mathbf{M}^*\ddot{\mathbf{q}}(t)+\mathbf{C}^*\dot{\mathbf{q}}(t)+\mathbf{K}^*\mathbf{q}(t))e^{-i\Omega t}dt \;=\; \int_{-\infty}^{+\infty}\mathbf{f}^*(t)e^{-i\Omega t}dt \qquad \text{(II.2.15)}$$

$$\mathbf{M}^*(-\Omega^2\mathcal{Q}(\Omega))+\mathbf{C}^*(i\Omega\mathcal{Q}(\Omega))+\mathbf{K}^*\mathcal{Q}(\Omega) \;=\; \mathcal{F}^*(\Omega) \qquad \text{(II.2.16)}$$

where

$$\mathcal{Q}(\Omega)=\int_{-\infty}^{+\infty}\mathbf{q}(t))e^{-i\Omega t}dt \;\text{ and }\; \mathcal{F}^*(\Omega)=\int_{-\infty}^{+\infty}\mathbf{f}^*(t))e^{-i\Omega t}dt \qquad \text{(II.2.17)}$$

It is worth noticing that in the discrete version of the Fourier transform, the maximum frequency that can be represented is defined as the Nyquist frequency. It is equal to half of the frequency sample as shown on the figure II.2.1.

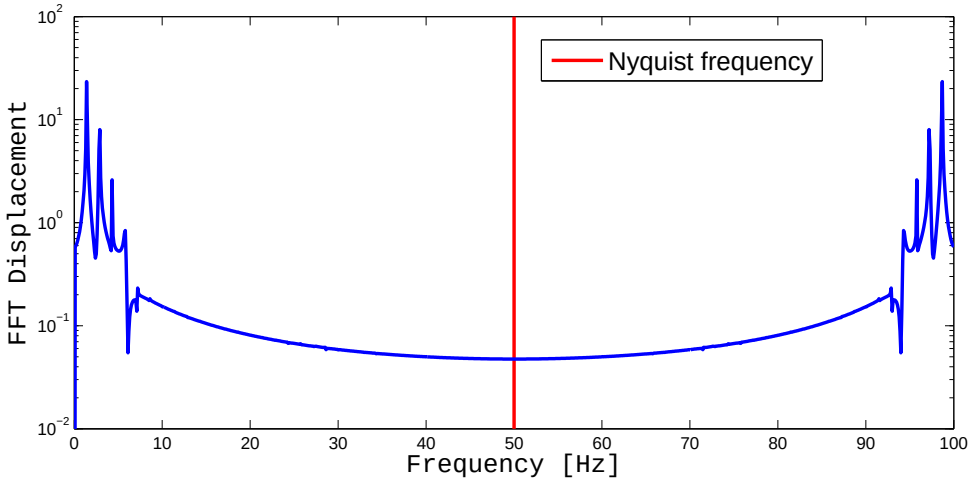

Figure II.2.1: Representation of the Nyquist frequency

This property of the Fourier transform will have an involvement when using the modal decomposition in the stochastic analysis. It is discussed more in detail afterwards.

The equation (II.2.16) can be rewritten in a simpler way using the fundamental property of the system called the transfer function,

$$\mathcal{Q}(\Omega)=\mathcal{H}^*(\Omega)\mathcal{F}^*(\Omega) \qquad \text{(II.2.18)}$$

where

$$\mathcal{H}^*(\Omega)=(-\mathbf{M}^*\Omega^2+\mathbf{C}^*i\Omega+\mathbf{K}^*)^{-1}. \qquad \text{(II.2.19)}$$

Once the displacement as a function of the frequency is obtained, the displacement as a function of time can be calculated using the inverse Fourier transform.

The result might be slightly different from the time domain analysis in the unsteady state because of the initial conditions. Indeed, it is not possible to impose an initial condition in the frequency analysis.

2.3 Stochastic approach

Beside the deterministic approach, the whole structural analysis can be done in a stochastic approach. However, the kind of results obtained from both analyses are slightly different on the form. Indeed, the deterministic approach provides a specific evolution of the displacement over time. The displacement is fully determined with the pressure field and the structural properties.

On the other hand, the stochastic approach gives the probabilistic properties of the structural response. In other words, the result of the analysis is not a specific evolution of the displacement over time but properties from which it is possible to generate different displacement fields with the same characteristics of the deterministic one.

2.3.1 Power spectral density

A stochastic process represents the evolution of random values over time. It can be defined by its probability density function of order 1, $\mathbf{p}_f(x,t)dx$, which expresses the probability that the function f takes a value between x and $x+dx$ at the time t.

The usual way of defining a stochastic process is to use the moments. The two first are:

- Mean

$$\mu_x(t) = E[x(t)] = \int_{-\infty}^{-\infty} x\mathbf{p}_x(x,t)dx \tag{II.2.20}$$

- Autocorrelation

$$\mathbf{R}_{xx}(t_1,t_2) = E[\mathbf{x}(t_1),\mathbf{x}(t_2)] = \int_{-\infty}^{+\infty}\int_{-\infty}^{+\infty} x_1x_2\mathbf{p}_x(x_1,t_1;x_2,t_2)dx_1dx_2. \tag{II.2.21}$$

These moments are really important because in a Gaussian process, they are enough to characterized it completely. Using directly these moments is difficult because the probability density function needs to be defined.

Moreover, most of the time, we do not have at our disposal many processes. Hopefully, the ergodicity theorem allows us to use only one sample that is long enough to represent it in an accurate way.

The autocorrelation can be rewritten,

$$\mathbf{R}_{xx}(\Delta t) = \lim_{T\to\infty}\int_{-T/2}^{+T/2} \mathbf{x}(t)\mathbf{x}(t+\Delta t)dt. \tag{II.2.22}$$

This equation leads us to an important function, the **power spectral density**. The PSD represents the frequency distribution of the energy from the stochastic process. It is defined as the Fourier transform of the autocorrelation,

$$\mathbf{S}_{xx}(\omega) = \frac{1}{2\pi}\int_{-\infty}^{+\infty} \mathbf{R}_{xx}(\tau)e^{-j\omega\tau}d\tau. \tag{II.2.23}$$

The PSD can also be express in the following way,

$$\mathbf{S}_{xx}(\omega) = \lim_{T\to\infty} \frac{2\pi}{T} E[|\mathbf{X}_i(\omega, T)|^2] \tag{II.2.24}$$

where $\mathbf{X}_i(\omega, T) = \frac{1}{2\pi}\int_{-T/2}^{+T/2} \mathbf{x}_i(t)e^{-j\omega t}dt$ is the Fourier transform of the truncated samples.

Again, only one sample can be used thanks to the ergodicity theorem:

$$\mathbf{S}_{xx}(\omega) = \lim_{T\to\infty} \frac{2\pi}{T} |\mathbf{X}_i(\omega, T)|^2. \tag{II.2.25}$$

The first fundamental property of the power spectral density is that its integral is equal to the variance of the process. Indeed, the autocorrelation and the PSD form a Fourier pair, the equation (II.2.23) and the inverse:

$$\mathbf{R}_{xx}(\tau) = \int_{-\infty}^{+\infty} \mathbf{S}_{xx}(\omega)e^{-j\omega\tau}d\omega. \tag{II.2.26}$$

If τ is replaced by 0, the equation becomes:

$$\mathbf{R}_{xx}(0) = \int_{-\infty}^{+\infty} \mathbf{S}_{xx}(\omega)d\omega = \sigma_x^2. \tag{II.2.27}$$

In practice, several random processes have to be considered. The definition of the PSD needs to be extended to the cross power spectral density:

$$\mathbf{S}_{xy}(\omega) = \lim_{T\to\infty} \frac{2\pi}{T} \mathbf{X}(\omega)\overline{\mathbf{Y}(\omega)} \tag{II.2.28}$$

which gives the covariance when integrated:

$$\int_{-\infty}^{+\infty} \mathbf{S}_{xy}(\omega)d\omega = \rho_{xy}\sigma_x\sigma_y. \tag{II.2.29}$$

It is possible to go one step further and to define the power spectral density matrix which contains all the PSD and cross-PSD of a whole set of random processes. Starting from a vectorial process containing different random processes, its Fourier transform can be computed:

$$\mathbf{x}(t) = \begin{pmatrix} \mathbf{x}_1(t) \\ \mathbf{x}_2(t) \\ \vdots \\ \mathbf{x}_n(t) \end{pmatrix} \quad \underset{\text{Fourier transform}}{\Longleftrightarrow} \quad \mathbf{X}(\omega) = \begin{pmatrix} \mathbf{X}_1(\omega) \\ \mathbf{X}_2(\omega) \\ \vdots \\ \mathbf{X}_n(\omega) \end{pmatrix}.$$

Using the definition given by the equation (II.2.28). The PSD matrix can be written:

$$\mathbf{S}_X = \lim_{T\to\infty} \tfrac{2\pi}{T}\mathbf{X}\overline{\mathbf{X}}^T = \begin{pmatrix} \mathbf{S}_{x_1}(\omega) & \mathbf{S}_{x_{12}}(\omega) & \dots & \mathbf{S}_{x_{1n}}(\omega) \\ \mathbf{S}_{x_{21}}(\omega) & \mathbf{S}_{x_2}(\omega) & \dots & \mathbf{S}_{x_{2n}}(\omega) \\ \vdots & \vdots & \ddots & \vdots \\ \mathbf{S}_{x_{n1}}(\omega) & \mathbf{S}_{x_{n2}}(\omega) & \dots & \mathbf{S}_{x_n}(\omega) \end{pmatrix}.$$

This important matrix contains a lot of information. By integration, the covariance matrix is obtained:

$$\int_{-\infty}^{+\infty} \mathbf{S}_X(\omega)d\omega = \begin{pmatrix} \sigma_{x_1}^2 & \rho_{12}\sigma_{x_1}\sigma_{x_2} & \dots & \rho_{1n}\sigma_{x_1}\sigma_{x_n} \\ \rho_{12}\sigma_{x_1}\sigma_{x_2} & \sigma_{x_2}^2 & \dots & \rho_{2n}\sigma_{x_2}\sigma_{x_n} \\ \vdots & \vdots & \ddots & \vdots \\ \rho_{1n}\sigma_{x_1}\sigma_{x_n} & \rho_{2n}\sigma_{x_2}\sigma_{x_n} & \dots & \sigma_{x_n}^2 \end{pmatrix}.$$

This matrix is the reference comparison point of this work. It could be expressed in terms of nodal or modal displacement.

In order to use it to solve structural problems, a mathematical property of the PSD needs to be defined.

Considering vectorial stochastic process $\mathbf{x}(t)$ with its corresponding PSD, $\mathbf{S}_x(\omega)$. The PSD of an other process $\mathbf{y}(t)$ defined by:

$$\underbrace{\mathbf{y}(t)}_{m\times 1} = \underbrace{\mathbf{A}}_{m\times n}\underbrace{\mathbf{x}(t)}_{n\times 1}. \tag{II.2.30}$$

is written

$$\underbrace{\mathbf{S}_y(\omega)}_{m\times m} = \underbrace{\mathbf{A}}_{m\times n}\underbrace{\mathbf{S}_x(\omega)}_{n\times n}\underbrace{\mathbf{A}^T}_{n\times m}. \tag{II.2.31}$$

The same relation can be defined in the frequency domain.

2.3.2 Resolution of the system

The starting point of the analysis is always the evolution of pressure over time. The first option is to compute directly the PSD of these pressure.

$$\mathbf{S}_p(\omega) = \lim_{T\to\infty} \frac{2\pi}{T}\mathbf{P}(\omega)\overline{\mathbf{P}(\omega)}^T. \tag{II.2.32}$$

The equation (II.1.2) expresses the relation between the pressure and the nodal forces. Using equation (II.2.31), it can be written:

$$\mathbf{S}_F(\omega) = \mathbf{A}\mathbf{S}_p(\omega)\mathbf{A}^T. \tag{II.2.33}$$

which gives the power spectral density of the nodal forces. The modal decomposition is applied to reduce the size of the system (equation (II.2.6)):

$$\mathbf{S}_{F^*}(\omega) = \boldsymbol{\phi}^T \mathbf{S}_F(\omega) \boldsymbol{\phi}. \tag{II.2.34}$$

Once the modal forces are known, the modal displacement is calculated using the function transfer as defined in equation II.2.35:

$$\mathbf{S}_q(\omega) = \mathbf{H}^*(\omega) \mathbf{S}_{F^*}(\omega) \overline{\mathbf{H}^*}^T(\omega). \tag{II.2.35}$$

This matrix contains the information needed to characterize the response of the structure. Particularly, it is possible to integrate it to obtain the modal correlation matrix.

The displacement in the modal basis can be projected the nodal one:

$$\mathbf{S}_x(\omega) = \boldsymbol{\phi} \mathbf{S}_q(\omega) \boldsymbol{\phi}^T \tag{II.2.36}$$

and eventually, it is possible to generate a displacement as a function of time from the PSD, using the frequency decomposition:

$$\mathbf{X}(\omega) = \sqrt{\frac{2\pi N}{\Delta t} \mathbf{S}_X(\omega)} e^{j\phi(\omega)} \tag{II.2.37}$$

where $\boldsymbol{\phi}(\omega)$ is a random phase shift. This value expresses the fact that the generated process is not unique.

Alternative method

The main problem using this general method is numerical. Indeed, the computation of the PSD matrix of the pressure is time and memory consuming.

The alternative way is to work with the pressure and the forces as a function of time until the modal forces are calculated. At this point, the PSD of the modal forces is evaluated. Depending on the number of modes kept, the size of the PSD matrix is drastically reduced.

This method is used in this work.

2.3.3 Background/Resonant decomposition

The next theoretical aspect discussed is the decomposition of the modal displacement PSD in two independent components, the background, which corresponds to the quasi static response and the resonant.

The first statistical moment is written:

$$\boldsymbol{\sigma}_q^2 = \int_{-\infty}^{+\infty} |\omega|^0 \mathbf{S}_q(\omega) d\omega. \tag{II.2.38}$$

It can be shown by mathematical development that the moments can be expressed by the sum of two terms:

$$\boldsymbol{\sigma}_q^2 = \underbrace{\int_{-\infty}^{+\infty} \frac{1}{\mathbf{K}^2}\mathbf{S}_{f^*}(\omega)d\omega}_{m_B} + \underbrace{\int_{-\infty}^{+\infty} (|\mathbf{H}(\omega)|^2 - \frac{1}{\mathbf{K}^2})\mathbf{S}_{f^*}(\omega)d\omega}_{m_R}. \tag{II.2.39}$$

The first term defines the background component, which is the moment of the modal force divided by the stiffness. The second term can be approximated such that the equation (II.2.39) is rewritten:

$$\boldsymbol{\sigma}_q^2 = \frac{\boldsymbol{\sigma}_{f^*}}{\mathbf{K}^2} + \frac{\mathbf{S}_{f^*}(\omega_{nat})}{\mathbf{K}^2}\frac{\pi\omega_{nat}}{2\xi}. \tag{II.2.40}$$

The interest of this expression is that the resonant component is calculated by knowing the value of the PSD of the modal forces only at the natural frequencies. When we are looking at partial measurements, a step of reconstruction of the missing data takes place. Thanks to this simplification, the reconstruction is used only for a few natural frequencies. Without this, it is unconceivable, regarding to time it takes, to apply this method numerically.

Modal correlation

The development made above could be extended to the cross PSD in order to obtain an expression of the modal cross correlation.

Considering two modes, m and n, their covariance can be written as a sum of a background and a resonant term, $C_{q_{mn}} = B_{mn} + R_{mn}$. The mathematics behind this formula is not discussed. Eventually, the complete equation is written:

$$C_{q_{mn}} = \frac{C_{f^*_{mn}}}{K^*_{mm}K^*_{nn}} + \frac{\pi\sqrt{\omega_m\omega_n}}{2\sqrt{\xi_m\xi_n}}\frac{\sqrt{S_{f^*_{mn}}(\omega_m)S_{f^*_{mn}}(\omega_n)}}{K^*_{mm}K^*_{nn}}\phi(\omega_m,\omega_n,\xi_m,\xi_n) \tag{II.2.41}$$

where

$$\phi(\omega_m,\omega_n,\xi_m,\xi_n) = \frac{8(\omega_m\omega_n)^{3/2}(\xi_m\omega_m + \xi_n\omega_n)\sqrt{\xi_m\xi_n}}{(\omega_m^2-\omega_n^2)^2 + 4\omega_m\omega_n(\xi_m\omega_m + \xi_n\omega_n)(\xi_m\omega_n + \xi_n\omega_m)} \tag{II.2.42}$$

is a natural frequency separation indicator because of the term $(\omega_m^2 - \omega_n^2)^2$ appearing in the denominator.

This equation is consistent with the expression of the background/resonant variance in equation II.2.40. Indeed, when $m = n$, both equations provide the same results.

Is it also possible to define the correlation coefficients. The development made consists in expressing the correlation coefficients as a weighted combination of a background and a resonant correlation:

$$\rho^q_{mn} = \gamma_B\frac{B_{mn}}{\sqrt{B_{mm}B_{nn}}} + \gamma_R\frac{R_{mn}}{\sqrt{R_{mm}R_{nn}}} \tag{II.2.43}$$

where γ_B and γ_R are two weighting coefficients defined by the background-to-resonant ratio in mode k, $b_k = B_{kk}/R_{kk}$:

$$\begin{cases} \gamma_B = & \dfrac{1}{\sqrt{1+b_m^{-1}}\sqrt{1+b_n^{-1}}} \\ \gamma_R = & \dfrac{1}{\sqrt{1+b_m}\sqrt{1+b_n}}. \end{cases} \tag{II.2.44}$$

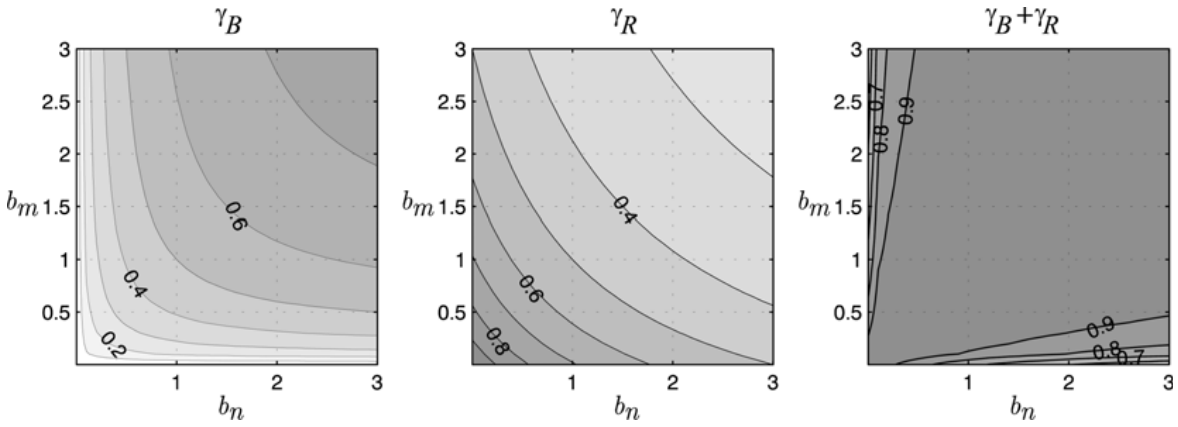

Figure II.2.2: Background (γ_B) and resonant (γ_R) weighting coefficients, as a function of the background-to-resonant ratios (b_m b_n)

To explain the meaning of equation II.2.43, it worth writing it in the following way:

$$\rho_{mn}^{q} = \gamma_B \rho_{mn}^{f^*} + \gamma_R \overline{\Gamma_{mn}} \phi(\omega_m, \omega_n, \xi_m, \xi_n). \tag{II.2.45}$$

Thus, the correlation coefficient is estimated by a weighted combination of the correlation of the generalised forces $\rho_{mn}^{f^*}$ and a dynamic correlation coefficient $\overline{\Gamma_{mn}}\phi(\omega_m, \omega_n, \xi_m, \xi_n)$.

In the limit case of a background response in both modes, $\gamma_B \approx 1$ and $\gamma_R \approx 0$ so that the response is quasi-static and the correlation of the modal responses is equal to that of the generalised forces. On the other limit case, a resonant response in both modes, $\gamma_B \approx 0$ and $\gamma_R \approx 1$ so that the correlation of the modal responses is defined by the resonant term $\overline{\Gamma_{mn}}\phi(\omega_m, \omega_n, \xi_m, \xi_n)$.

Chapter 3

Singular Value Decomposition

The Singular Value Decomposition is useful for the reconstruction of missing data. It is a factorisation tool for real or complex rectangular matrix. The general form of the SVD is:

$$\underbrace{\mathbf{M}}_{m\times n} = \underbrace{\mathbf{U}}_{m\times m}\underbrace{\mathbf{\Sigma}}_{m\times n}\underbrace{\overline{\mathbf{V}}^T}_{n\times n} \tag{II.3.1}$$

where $\mathbf{U}$ and $\mathbf{V}$ are unitary matrices and $\mathbf{\Sigma}$ is a diagonal matrix with non-negative real numbers on the diagonal. The idea of this factorization is similar to the eigenvalue decomposition, expressing the main directions of a matrix in terms of singular values and vectors.

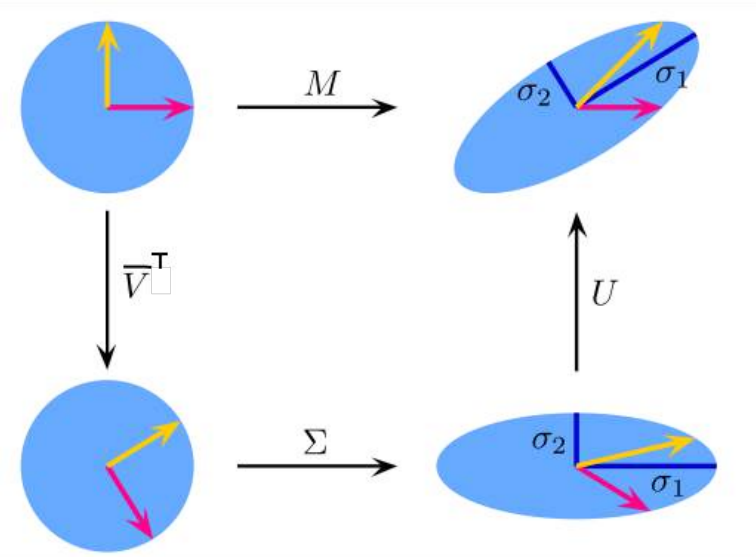

Figure II.3.1: Processus of the singular value decomposition

It is worth illustrating the principle with a simple example where M is a $[3 \times 2]$ matrix:

$$\underbrace{\begin{pmatrix} m_{11} & m_{12} \\ m_{21} & m_{22} \\ m_{31} & m_{32} \end{pmatrix}}_{\mathbf{M}} = \underbrace{\begin{pmatrix} | & | & | \\ \mathbf{u}_1 & \mathbf{u}_2 & \mathbf{u}_3 \\ | & | & | \end{pmatrix}}_{U} \underbrace{\begin{pmatrix} \sigma_1 & 0 \\ 0 & \sigma_2 \\ 0 & 0 \end{pmatrix}}_{\mathbf{\Sigma}} \underbrace{\begin{pmatrix} -\overline{\mathbf{v}_1}- \\ -\overline{\mathbf{v}_2}- \end{pmatrix}^T}_{\overline{\mathbf{V}}^T}. \tag{II.3.2}$$

The σ_i represents the singular values and the $\mathbf{u}_i$ the singular vectors. Using the properties of the eigenvalue decomposition, it is possible to generate a $m \times m$ matrix, $\hat{\mathbf{M}}$. This matrix have as property that its n first principal directions are similar to the one of $\mathbf{M}$. The generation is made using the n singular values and vectors:

$$\underbrace{\hat{\mathbf{M}}}_{m \times m} = \underbrace{\widetilde{\mathbf{U}}}_{m \times n} \underbrace{\widetilde{\mathbf{\Sigma}}}_{n \times n} \underbrace{\widetilde{\mathbf{U}}^T}_{n \times m} \tag{II.3.3}$$

where $\widetilde{\mathbf{U}}$ is a $m \times n$ matrix extracted from $\mathbf{U}$ with the n first singular vectors in the columns and $\widetilde{\mathbf{\Sigma}}$ is a $n \times n$ matrix extracted from $\mathbf{\Sigma}$ with the n singular values on the diagonal.

Part III

Reference Model Analysis

Chapter 1

Model properties

The reference analysis consists in applying a standard approach on which we can rely on in order to get results that could be compared afterwards. It is really important to be confident in the method and on its results because the conclusion we will be based on them.

The first step is to define the properties of the model that is used.

1.1 Experimental Data

The results from *Kikuchi & al.* experiment are given in terms of pressure coefficient, $\mathbf{c}_p(t)$. The pressures measured are divided by a factor K in such a way that the $\mathbf{c}_p(t)$ obtained are dimensionless:

$$\mathbf{c}_p(t) = \frac{\mathbf{p}(t)}{K_{ref}} \tag{III.1.1}$$

where $K_{ref} = \frac{1}{2}\ \rho\ U_{ref}^2$.

In order to get results in terms of physical values, we work directly with pressures (i.e. in $\frac{N}{m^2}$) instead of pressure coefficients. Moreover, as the reference wind speed used in the experiment (21.2 m/s) was lower than traditional design wind speed, we will scale the measured pressure to a wind speed of 30 m/s.

$$\mathbf{p}(t) = \mathbf{c}_p(t)\ K_{ref}\ \frac{U_{design}^2}{U_{ref}^2} \tag{III.1.2}$$

1.2 Finite element model

A straight-line model is used to represent the reference building. The model thus have the behaviour of a free-fixed beam. This choice is reasonable for two reasons. Firstly, the ratio between the height and the width, $\frac{h}{b} = 5$, is large. Secondly, the pressure coefficients from the experiment are independent of the structural properties of the building. It

means that the mass, the stiffness and the damping ratio of our model need to be defined. To stay focus on the motivation of this work, which must be as general as possible, we did not try to calculate structural properties using a specific building. Indeed, using a line model allows us to work with structural properties integrated over the area and thus not related to a specific building configuration.

In order to be consistent with the available data, a model with 25 elements and 26 nodes is used. The resultant pressure is measured in the middle of each element. This pressure will be considered as constant along the element.

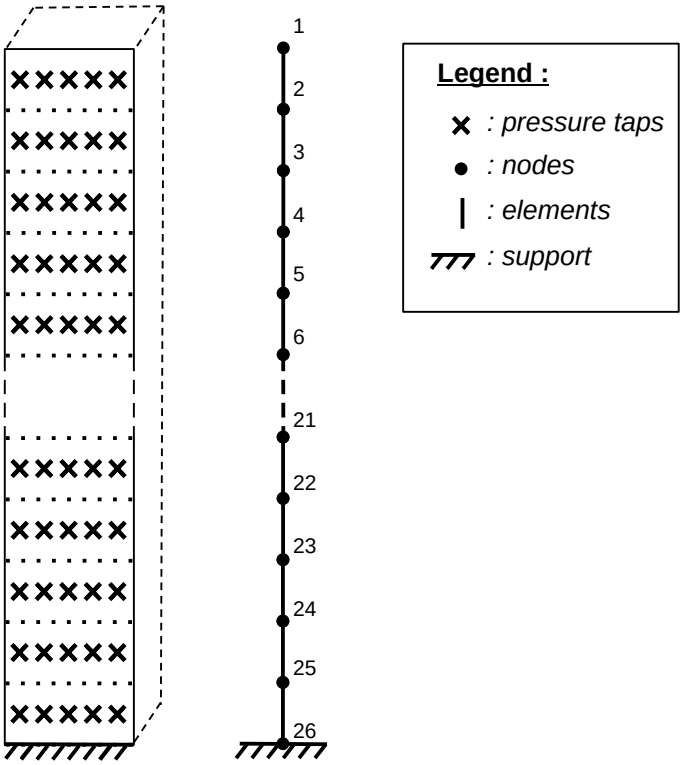

Figure III.1.1: Finite element model

Since each nodes has 5 degrees of freedom, the total number of *dof* of the model is 130. The projection of the pressure into nodal forces is made by the intermediate of the influence matrix, A. It integrates the pressure over the influence area and calculates the work equivalent forces. Considering $\mathbf{P}_i(t)$, the pressure on the face i, it can be written:

$$\underbrace{\begin{pmatrix} \mathbf{F}_X(t) \\ \mathbf{F}_Y(t) \\ \mathbf{M}_Z(t) \\ \mathbf{M}_X(t) \\ \mathbf{M}_Y(t) \end{pmatrix}}_{N_{dof}\times N_t} = \underbrace{\begin{pmatrix} \mathbf{A}_X & \mathbf{O} & -\mathbf{A}_X & \mathbf{O} \\ \mathbf{O} & \mathbf{A}_Y & \mathbf{O} & -\mathbf{A}_Y \\ \mathbf{A}_{M_Z} & \mathbf{A}_{M_Z} & \mathbf{A}_{M_Z} & \mathbf{A}_{M_Z} \\ \mathbf{O} & \mathbf{A}_{M_X} & \mathbf{O} & -\mathbf{A}_{M_X} \\ \mathbf{A}_{M_Y} & \mathbf{O} & -\mathbf{A}_{M_Y} & \mathbf{O} \end{pmatrix}}_{N_{dof}\times N_{taps}} \underbrace{\begin{pmatrix} \mathbf{P}_1(t) \\ \mathbf{P}_2(t) \\ \mathbf{P}_3(t) \\ \mathbf{P}_4(t) \end{pmatrix}}_{N_{taps}\times N_t} \tag{III.1.3}$$

where N_{dof} is the number of degree of freedom of the system, N_t the number time samples and N_{taps} the number of pressure taps on the model.

The shape of the matrix is consistent with the physical behaviour, the crosswind pressure (faces 2 and 4) has no influence on the along-wind forces ($\mathbf{F}_X$ and $\mathbf{M}_Y$) and vice versa.

To take into account the boundary conditions, the dofs connected to the ground needs to be removed from the analysis. The foundation is not deformable so $\{\mathbf{x}_{ground}\}(t) = 0$. Once all the other displacements are known, the boundary conditions are added back to the results.

1.3 Structural properties

If the mass of a structure can be easily estimated, the stiffness is difficult to estimate in a simple way. In that purpose, we chose to fix the natural frequency of the first bending and torsional vibration modes. Indeed, with some experience and judgment it is easy to estimate them for high-rise building.

We use in this paper a first natural frequency of 0.2 Hz in the first flexion mode and of 2.5 Hz in the first torsional mode. To force the natural frequencies, we started from their definition:

$$\omega_{nat} = \sqrt{\frac{\mathbf{K}}{\mathbf{M}}}. \tag{III.1.4}$$

As we said, the easiest value to estimate is the mass. To define our mass matrix, we make an hypothesis on the linear mass, $\mu = 10,000 \frac{kg}{m}$.

Knowing the natural frequency we want to obtain, the only unknown left is the stiffness. As both the flexional and torsional stiffnesses are linear functions of a stiffness modulus times an inertia, these stiffnesses can be written in the following way:

$$\mathbf{K}_{flex} = f(EI) \tag{III.1.5}$$
$$\mathbf{K}_{tors} = f(GJ). \tag{III.1.6}$$

The system is linear, starting with an unitary stiffness, we can therefore obtain the targeted stiffness with a cross-multiplication. Eventually, the obtained stiffness are:

$$EI = 2.044.10^{12} N.m^2 \tag{III.1.7}$$
$$GJ = 6.665.10^{13} N.m^2. \tag{III.1.8}$$

As the structure is symmetric, the vibration modes along both the x and y axis are exactly the same. The figure B.14 shows the mode shapes of the first seven modes.

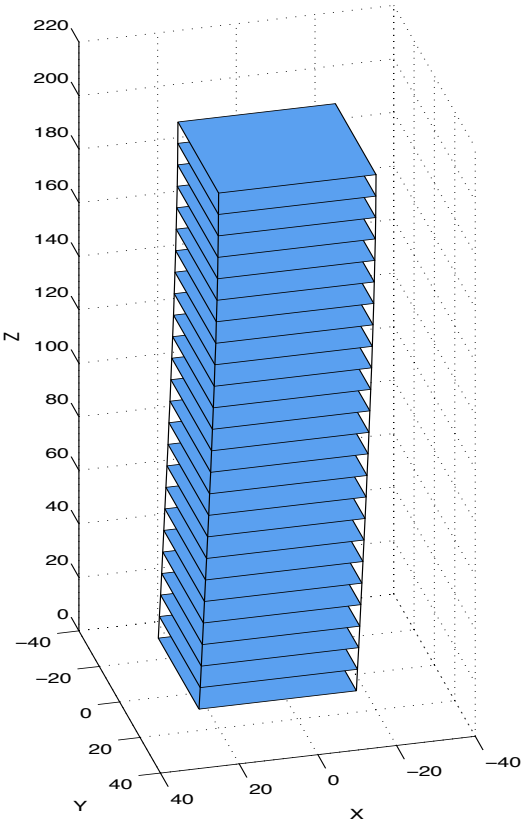

(a) 1^{st} and 2^{nd} modes

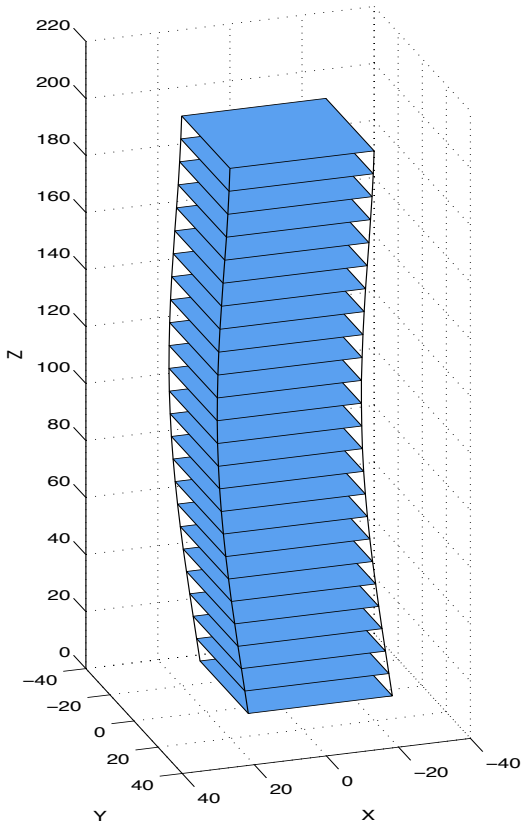

(b) 3^{rd} and 4^{th} modes

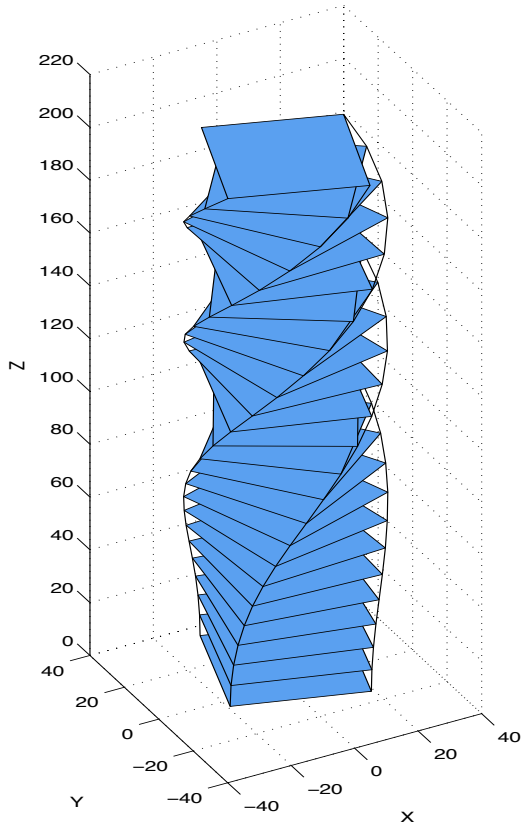

(c) 5^{th} mode

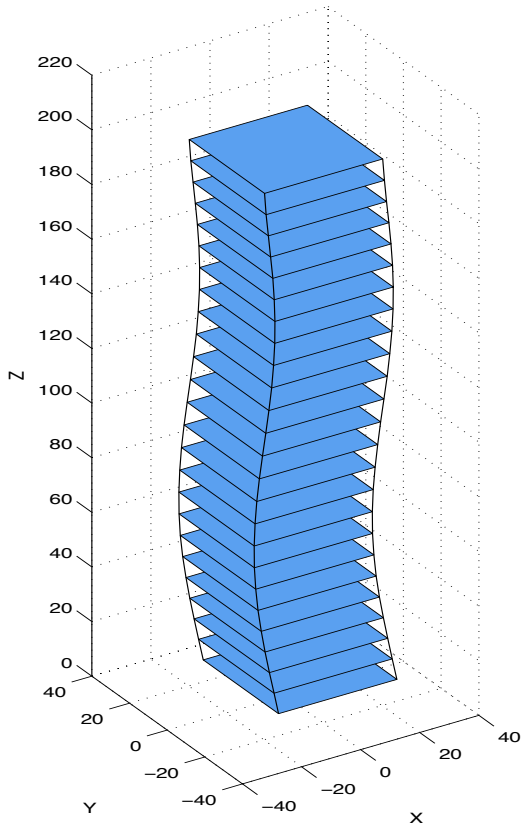

(d) 6^{th} and 7^{th} modes

Figure III.1.2: Mode shapes

The natural pulsation of these modes are given in the following table:

Mode	$B1-x$	$B1-y$	$B2-x$	$B2-y$	$T1$	$B3-y$	$B3-x$
$\omega\ [rad/s]$	1.26	1.26	7.88	7.88	15.71	22.05	22.05

Table III.1.1: Natural pulsation of the main modes.

where $B1-x$ is the bending mode in the x direction, $T1$ the first torsional mode, etc.

Concerning the damping matrix, the Rayleigh approximation is used. Since the mass and the stiffness matrices are known the only unknown left is the damping ratio, ξ. This value is chosen equal to 0.003, which is a standard value for buildings [6].

Chapter 2

Deterministic approach

In this chapter, the two deterministic methods discussed in the theoretical part are applied on the defined model. The objective of this is twofold. Firstly, to verify the consistence of the system by comparing the displacements gotten from the frequency domain and the time domain analysis. Secondly, to analyse the accuracy of the modal decomposition and the discrepancy as a function of the number of modes kept.

2.1 Comparison of the time domain and the frequency domain analysis

To illustrate the results, the displacements along x and y and the rotation at the top are represented on figure III.2.1.

It can be seen that the displacements are similar and fit perfectly each other in the stationary part. As expected, some discrepancy appears at the beginning in the unsteady state. This difference is due to the initial condition imposed in the time domain analysis.

The response of the structure is resonant as further discussed next. The extreme displacements for the different angles of attack are given in the following table.

	Wind incidence		
Displacement	0°	15°	45°
X direction $[mm]$	16.0	17.9	13.4
Y direction $[mm]$	40.5	23.3	13.4
Rotation $[10^{-9} rad/m]$	3.63	2.31	1.42

Table III.2.1: Maximum displacement at the top for different angles of attack.

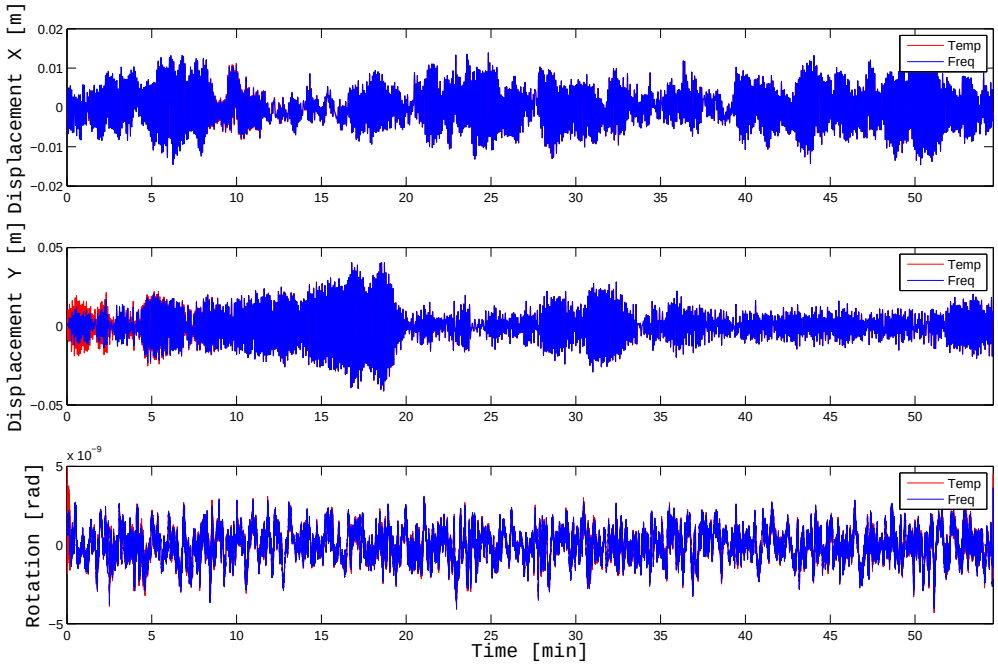

Figure III.2.1: Displacements at the top for a 0° angle of attack.

The obtained maximum displacements are small compared to usual deflections but they are related to the chosen properties of the model.

An interesting observation is that the displacement in the crosswind direction is more important than the displacement in the along-wind direction. This phenomena is due to the vortex shedding that solicits the structure laterally.

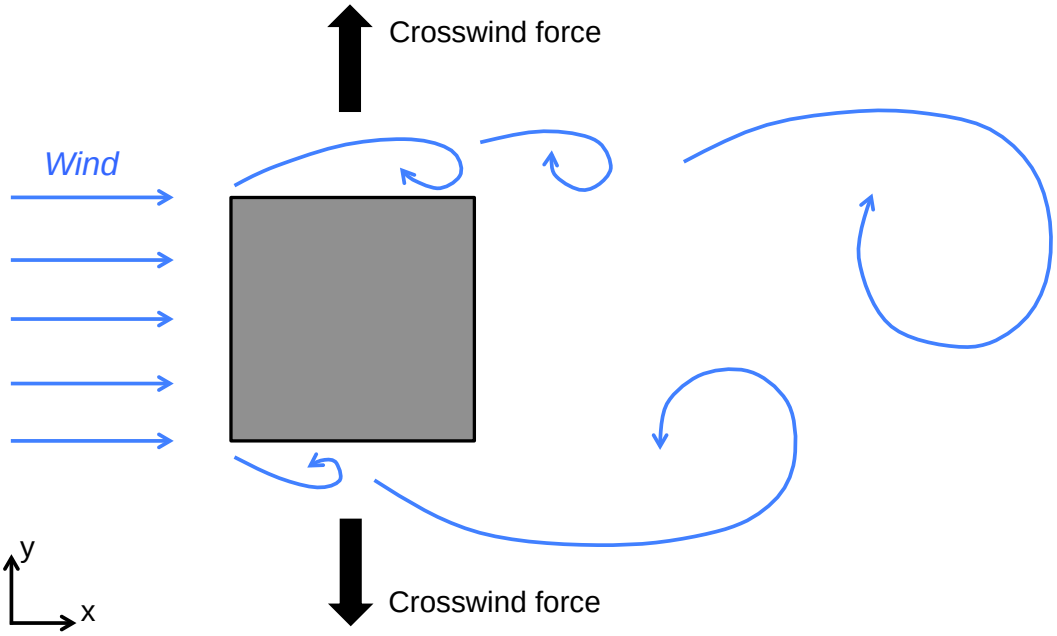

Figure III.2.2: Illustration of the vortex shedding phenomena on the building.

When the wind passes the building, the flow detaches itself from the structure and creates vortices in the wake. These vortices detachments occur in a periodic way at each side of the building, which means that crosswind forces appear and solicit the structure in the other direction.

The vortex shedding frequency is characterised by the *Strouhal* number:

$$St = \frac{f_v D}{U_{wind}} \tag{III.2.1}$$

where f_v is the frequency of vortex shedding, D is the characteristic length and U is the wind velocity. To validate that the vortex shedding is the cause of this observation, the frequency of the phenomena need to be found and compared to the PSD of the forces.

Several studies have been conducted to define the *Strouhal* number on square cylinders [8] & [9]. The range of the values starts from 0.12 to 0.16. The characteristic length is $40m$, the width of the building and U_{wind} is equal to 30 m/s. Finally, we obtain:

$$\omega_v = 2\pi f_v \in [0.61\ 0.84].$$

As it is discussed more in detail afterwards, the response in the Y-direction takes place mainly in the corresponding first mode. The PSD of the modal force in this mode can be computed:

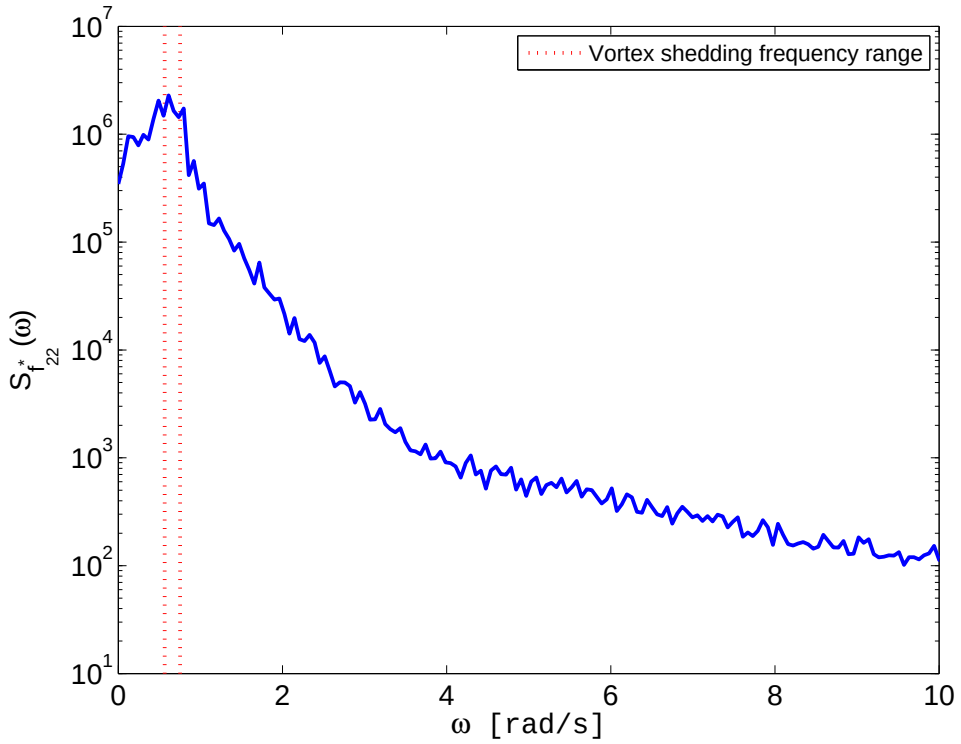

Figure III.2.3: PSD of the modal force in the first mode along y-axis.

It can be seen that most of the energy contained in the PSD of the modal forces is in the range of the vortex shedding frequency. This allows us to validate the hypothesis that the vortex shedding is the main reason of the crosswind forces applied on the building for a 0° angle of attack.

The response of the structure is resonant. It is thus interesting to characterise the intensity of the resonant phenomena by calculating the dynamic amplification factor. The DAF expresses the value by which the quasi-static deflections should be multiplied to obtain the deflections caused by a dynamic load. In other words it is the ratio between the value in the table III.2.1 and the maximum quasi-static displacement:

$$DAF = \frac{x_{max}}{x_{qs,max}}. \tag{III.2.2}$$

The DAF related to the along-wind and crosswind displacements are given in the following table:

Wind incidence	0°		15°		45°	
Direction	x	y	x	y	x	y
Dynamic displacement $[mm]$	16.0	40.5	17.9	23.2	13.4	13.4
Quasi-static displacement $[mm]$	6.5	7.0	5.4	7.1	4.3	4.2
DAF	2.47	5.80	3.34	3.29	3.11	3.20

Table III.2.2: Dynamic amplification factor along-wind and crosswind displacements for different angles of attack.

In the 0° angle of attack, the DAF is more important in the y-axis. It is the perfect illustration of the vortex shedding phenomena described above.

2.2 Accuracy of the modal decomposition of the quasi-static response.

As we said in the theoretical part, the modal decomposition is well adapted for resonant response but it might be less accurate for the quasi-static component. In order to quantify the discrepancy of the modal decomposition, we calculate the mean relative error of the maximum displacement for each degree of freedom between the displacement in the nodal basis and the displacement in modal basis using a different number of modes.

$$\begin{cases} \mathbf{x}_{Nodal}(t) = & \mathbf{K}^{-1}\mathbf{f}(t) \\ \mathbf{x}_{Modal}(t) = & \boldsymbol{\phi}\mathbf{K}^{*-1}\mathbf{f}^{*}(t) \end{cases} \tag{III.2.3}$$

The obtained errors are given in the following table:

Number of modes	0°			15°			45°		
	x	y	z	x	y	z	x	y	z
1	4.5	-	-	5.2	-	-	8.8	-	-
2	4.5	6.7	-	5.2	8.4	-	8.8	7.4	-
3	1.3	6.7	-	1.3	8.4	-	2.5	7.4	-
4	1.3	6.7	-	1.3	0.9	-	2.5	2.3	-
5	1.3	6.7	5.1	1.3	0.9	5.6	2.5	2.3	20.3
⋮	⋮	⋮	⋮	⋮	⋮	⋮	⋮	⋮	⋮
7	0.1	0.1	5.1	0.6	0.5	5.6	0.9	1.1	20.3
⋮	⋮	⋮	⋮	⋮	⋮	⋮	⋮	⋮	⋮
50	10^{-4}	10^{-3}	10^{-3}	10^{-3}	10^{-3}	10^{-2}	10^{-3}	10^{-3}	10^{-2}
⋮	⋮	⋮	⋮	⋮	⋮	⋮	⋮	⋮	⋮
125	10^{-10}	10^{-10}	10^{-12}	10^{-10}	10^{-10}	10^{-12}	10^{-10}	10^{-10}	10^{-12}

Table III.2.3: Relative error [%] for the maximum displacement using the modal decomposition with different number of modes

It can be seen in the table above that the relative errors decrease sharply when using more than 5 modes. Thus, it is considered that with 5 modes or more, the quasi-static response is well represented in the modal basis.

Chapter 3

Stochastic approach

This approach provides the reference results of our analysis. The path followed is explained in the section 2.3.2.

Starting from the pressure field on the model, the work-equivalent forces are calculated using the influence matrix defined in the section 1.2:

$$\mathbf{f}(t) = \mathbf{A}\mathbf{p}(t) \tag{III.3.1}$$

where $\mathbf{p}(t) = [500 \times N_t]$, $\mathbf{A} = [125 \times 500]$ and $\mathbf{f}(t) = [125 \times N_t]$.

The next step is to express these forces in a modal basis.

3.1 Modal decomposition

The PSD is expressed as a function of the pulsation from 0 to $\frac{\pi}{dt}$, the Nyqvist pulsation. It means that higher frequencies can not be represented. Comparing this maximum pulsation to the natural pulsation of our modes, we see that in only seven modes the natural pulsation is below.

To stay consistent with this observation, these seven modes are kept in the modal analysis. As it is shown in the deterministic approach, the error of the quasi static response in the modal basis using seven modes is small. It is thus reasonable to use the modal decomposition for the entire response.

The modal forces are calculated using the modal vectors:

$$\mathbf{f}^*(t) = \boldsymbol{\phi}^T \mathbf{f}(t) \tag{III.3.2}$$

where $\mathbf{f}(t) = [125 \times N_t]$, $\boldsymbol{\phi} = [125 \times 7]$ and $\mathbf{f}^*(t) = [7 \times N_t]$.

Following the alternative method described in the theoretical chapter in order to improve the numerical efficiency in terms of time, the PSD of the modal forces is computed.

3.2 Window function

As discussed in the theoretical chapter, a PSD can be compute from one sample using the ergodicity theorem. Practically, if the signal is long enough, a window function is used in order to get several smaller signals from the original one.

$$f^{*k}{}_{ij} = F^{k}_{windowj} f^{*}{}_{ij} \tag{III.3.3}$$

where k is the number of the window, i the number of the modal force and j the time abscissa. The window function used in this paper is a unitary rectangle that moves over the signal as illustrated in the figure below.

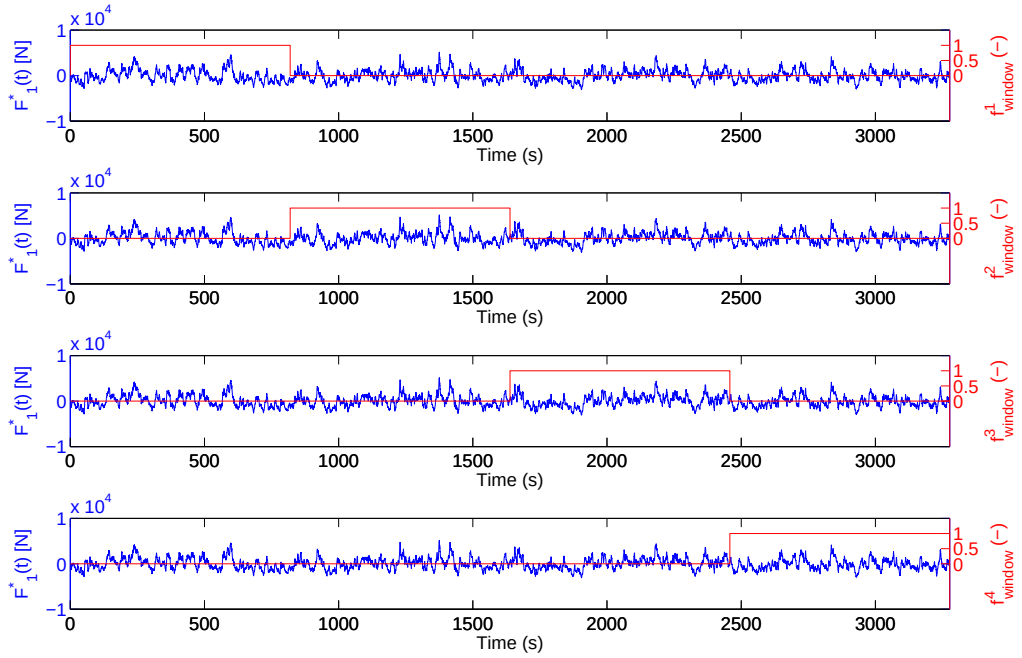

Figure III.3.1: Illustration of the window function principle.

For each windowed signal, a PSD is calculated. This technique has the advantage that an average can be made so that the noise in the final result is reduced. The figure III.3.2 illustrates the influence of the number of windows on the PSD.

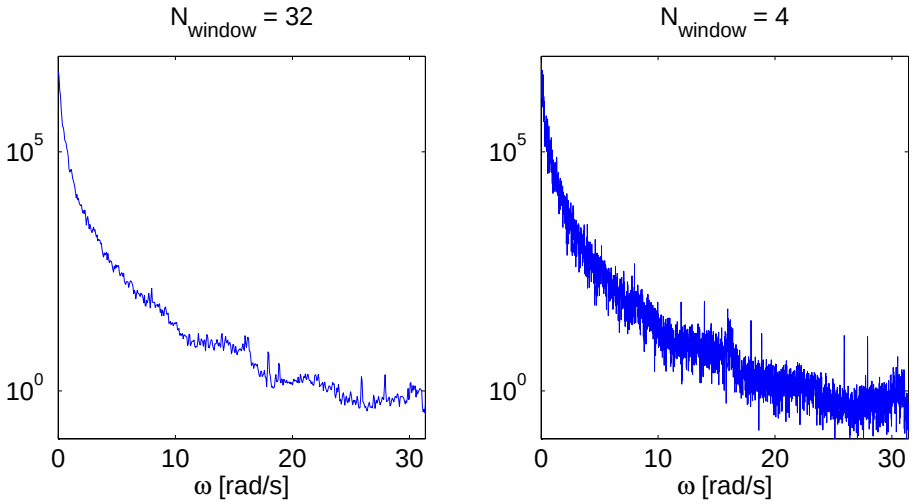

Figure III.3.2: Influence of the number of windows on the PSD.

Eventually, a window length of 1024 points is chosen in order to have a good compromise between the number of windows and the number of points in each window.

3.3 PSD and covariance matrices of the displacements

Using seven modes in the modal decomposition leads us to compute 7 PSD and 21 Cross-PSD (because of the symmetry) of the modal forces. The figure III.3.3 illustrates the PSD of the modal forces for the first three modes.

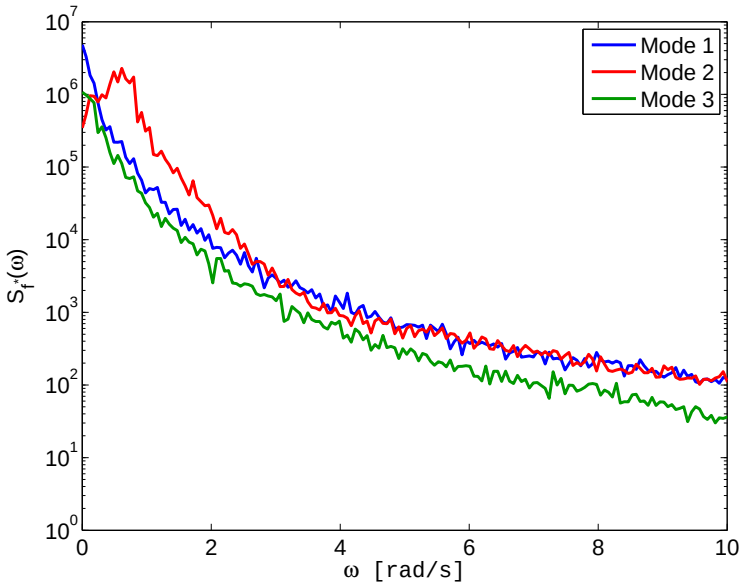

Figure III.3.3: PSD of the modal forces in the first three modes for an angle of attack of 0°

From this point, the PSD of the modal displacement can be calculated by post and pre multiplying the PSD of the modal forces by the transfer function of the system:

$$\mathbf{S}_q(\omega) = \mathbf{H}^*(\omega)\mathbf{S}_{F^*}(\omega)\overline{\mathbf{H}^*}^T(\omega) \tag{III.3.4}$$

which gives the PSD of the modal displacement in the first three modes shown on figure B.4,

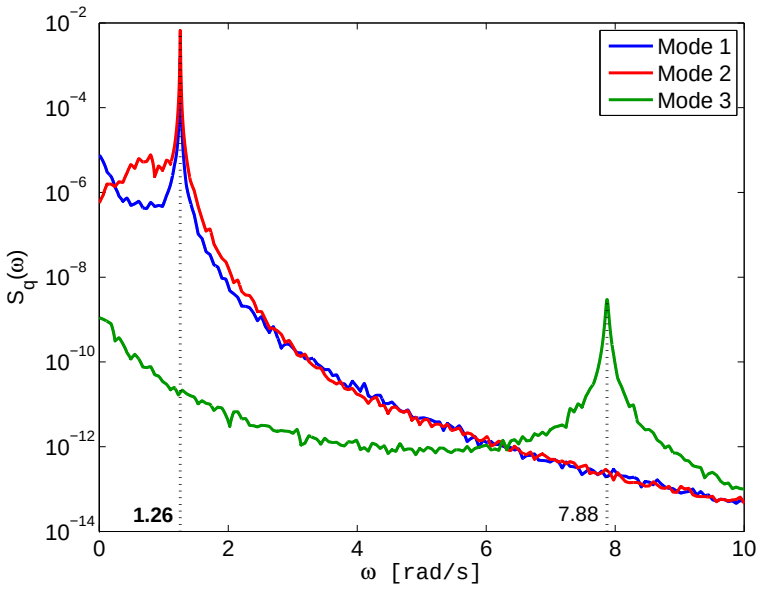

Figure III.3.4: PSD of the modal displacement in the first three modes for an angle of attack of 0°

One of the main interests of these PSDs is their integral. Indeed, by integrating the PSDs over the frequency, the covariance matrix is computed. To understand the meaning of this information, the diagonal that contains the variance or the standard deviation of the modal displacements is extracted and the complete matrix is normalised to a unitary diagonal in order to get the modal correlation coefficients.

These two are the comparison points of our analysis. It means that at the end of every approach, we compare the standard deviation and the modal correlation of the modal displacements in order to estimate any deviation occurring between the different processes.

The standard deviation of the modal displacements for each mode used in the analysis are given on figure III.3.5.

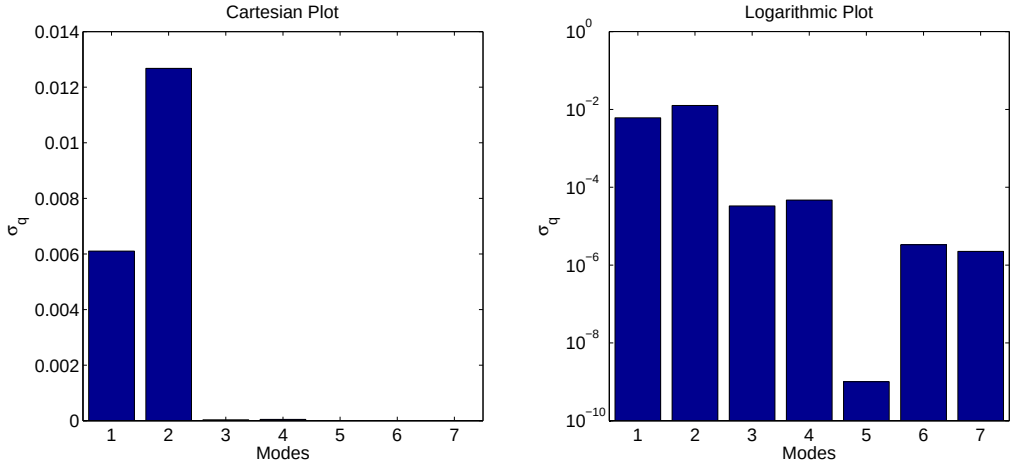

(a) Angle of attack of 0°.

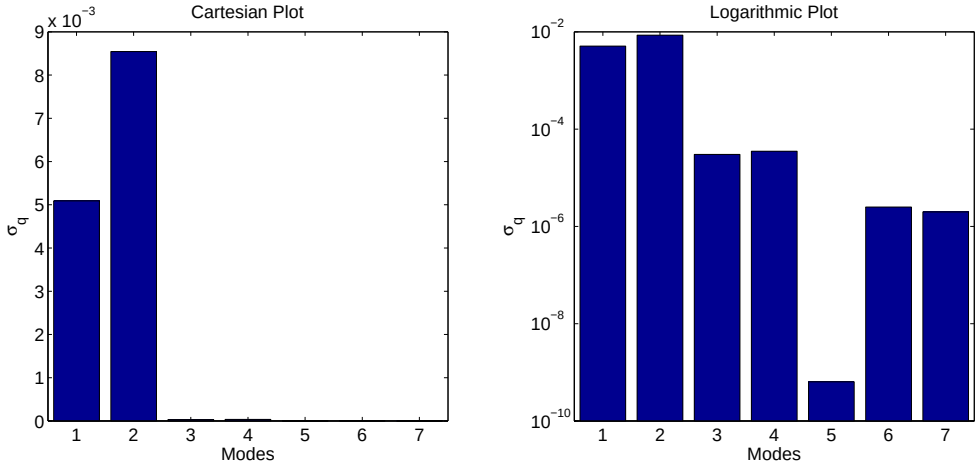

(b) Angle of attack of 15°.

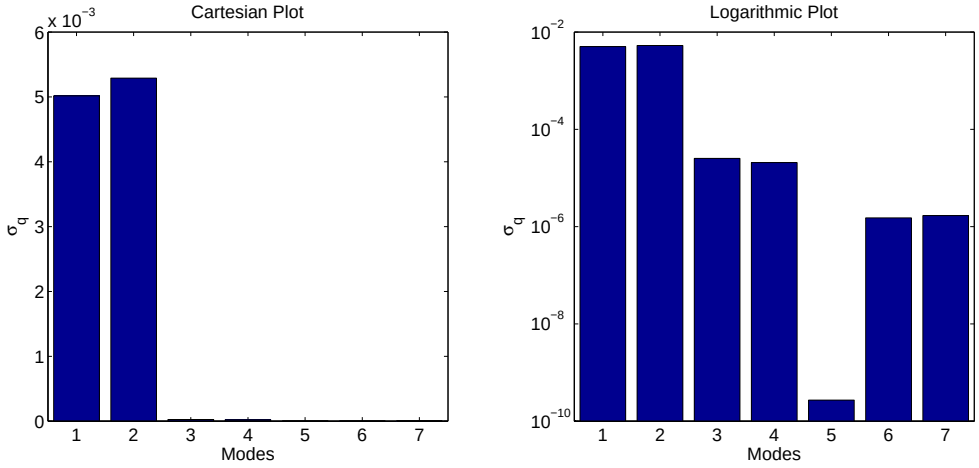

(c) Angle of attack of 45°.

Figure III.3.5: Standard deviation of the modal displacement in the first seven modes.

As it can be seen, the response takes place almost only in the first two modes for each angle of attack. This first observation have an important impact on the second

comparison point chosen. Indeed, as the variance is only important in the first two modes, comparing the modal correlation only makes sens between these two modes. In other words, from the matrix presented below, only one value is interesting to compare and quantify the accuracy of the reconstruction.

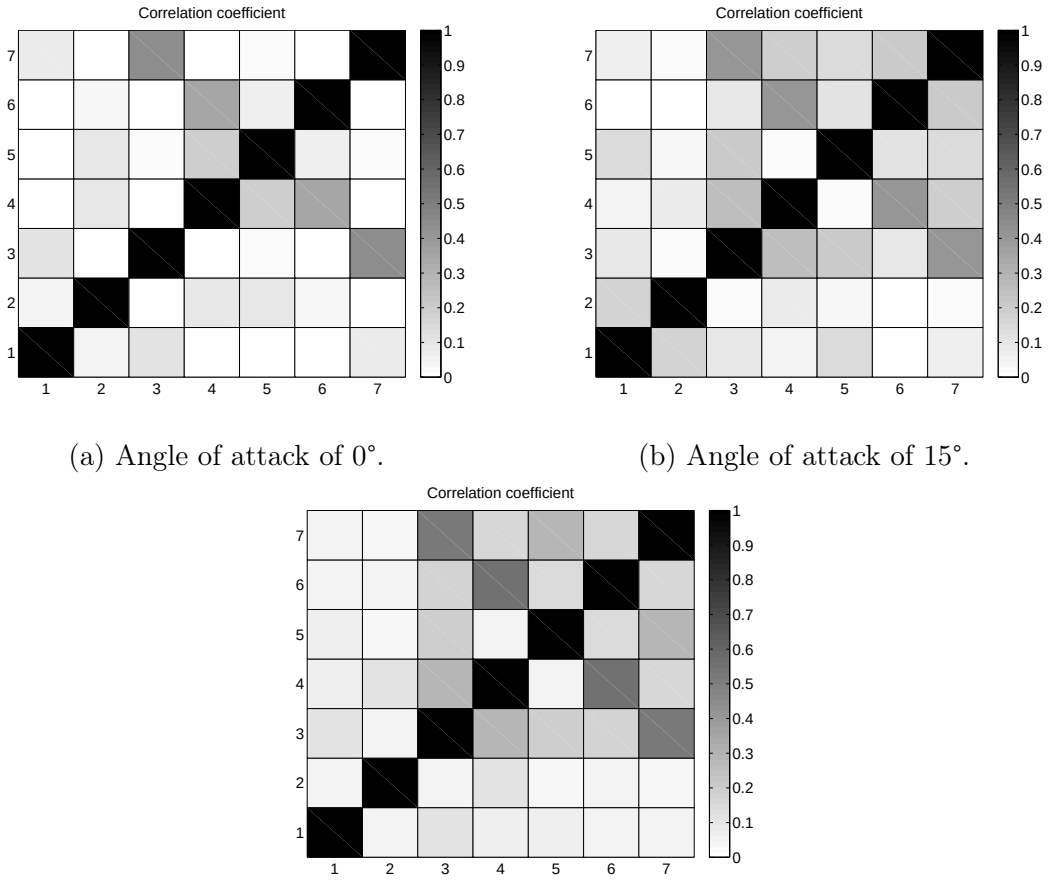

(a) Angle of attack of 0°.

(b) Angle of attack of 15°.

(c) Angle of attack of 45°.

Figure III.3.6: Correlation coefficient of the modal displacement.

The figure above represent the full correlation coefficient matrix for the three angles of attacks. It is presented for information since the only important value from this matrix is the correlation between the first and the second mode.

The correlation is relatively small for each mode. The higher correlation that appears is between the second and third modes both in the x and the y direction. It can also be seen that generally, the correlations are more important in the case of the angle of attack of 45°, which is explained by the symmetry of the loading between the two directions x and y.

Chapter 4

Background/Resonant decomposition

In this chapter, we apply the background/resonant decomposition in order to quantify the error made using this approach. The main idea of this method is to replace the response of a structure by two independent components, the quasi-static one and the resonant one.

4.1 Illustration of the Background/Resonant decomposition

The equation of the PSD using the background/resonant principle is written:

$$\mathbf{S}_q(\omega) = \underbrace{\frac{\mathbf{S}_{f^*}(\omega)}{\mathbf{K}^2}}_{Background} + \underbrace{\mathbf{S}_{f^*}(\omega_{nat})|\mathbf{H}(\omega)|^2}_{Resonant}. \tag{III.4.1}$$

To illustrate this decomposition, we apply it on the PSD of the modal displacement in the first mode. The component of S_q are plotted in order to compare them to the PSD from the complete stochastic analysis. The figure III.4.1 represents the PSD of the modal displacement in the first mode from the Background/Resonant decomposition. The curve in red is simply the sum of the two others.

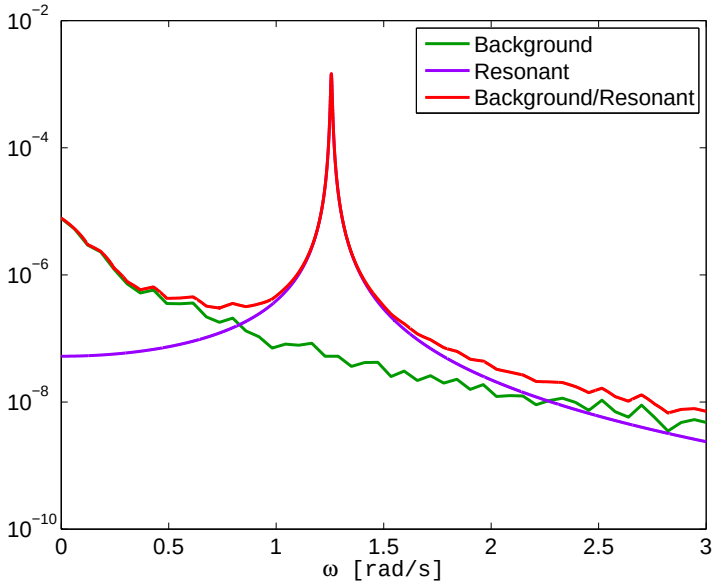

Figure III.4.1: Background/Resonant decomposition of PSD of the modal displacement in the first mode.

This curve is compared to the one obtained in the complete stochastic analysis and represented on figure III.3.4.

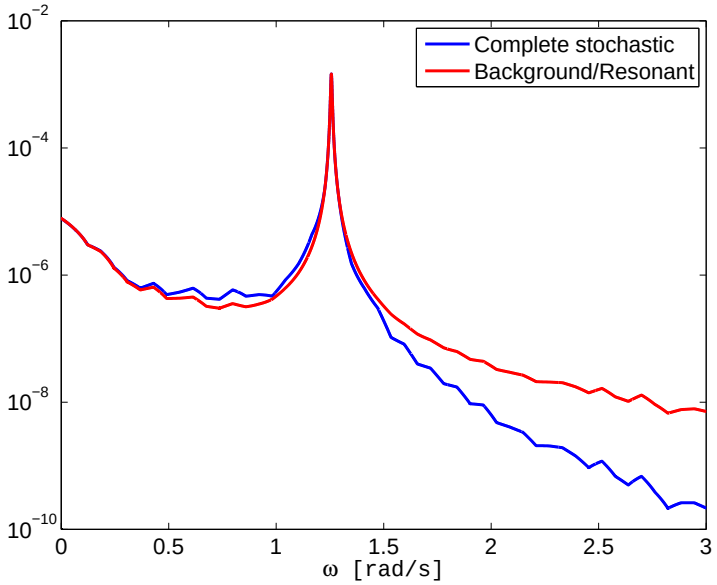

Figure III.4.2: Comparison of the PSD of the modal displacement in the first mode with B/R and complete stochastic analysis.

It can be seen that the curves are perfectly similar in the low frequency range and near the peak. These observations are easily explained because in these two frequency ranges, the response is mostly governed by one phenomenon, either the background or the resonant.

On the other hand, in between these two zones, the response is influenced by both components which means that the hypothesis of the independency between them is no longer valid. Hopefully, the interesting value is the integral of these curves. On a Cartesian plot, it can be seen that most of the energy is in the peak (III.4.3). That means that it is the part where the most accuracy is needed.

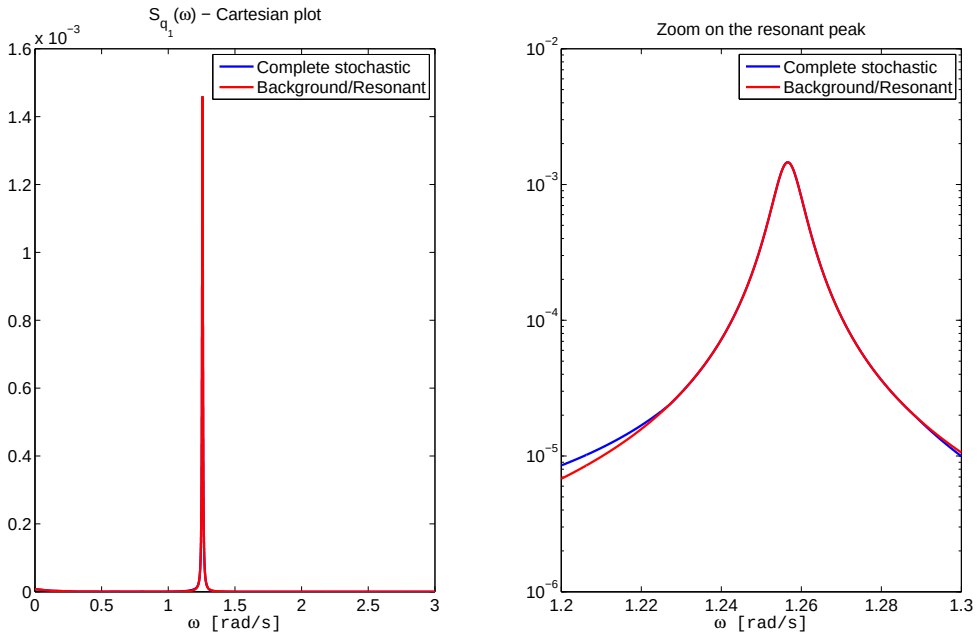

Figure III.4.3: PSD in a cartesian plot and zoom on the resonant peak.

The right figure represents a zoom on the resonant peak. The two curves are extremely close to each other.

This approach gives a good idea of the mechanism behind the background/resonant decomposition. However, it is not possible to rely on visual observations. To definitely validate this approach, these curves are integrated in order to have values to compare with the complete stochastic analysis. This integration provides us with the covariance matrix.

4.2 Covariance matrix of the modal displacements

The background/resonant decomposition is applied directly on the modal displacements:

$$\mathbf{q}_{BR}(t) \quad = \quad \mathbf{q}_B(t) + \mathbf{q}_R(t) \tag{III.4.2}$$

where $\mathbf{q}_B(t)$ is the background response and $\mathbf{q}_R(t)$ the resonant response.

To compare the results we work with the covariance matrices of the modal displacements. The covariance of a sum is written in the following way:

$$\mathbf{C}_{q_{BR}} = \mathbf{C}_{q_B} + \mathbf{C}_{q_R} + \mathbf{C}_{q_B,q_R}. \quad \text{(III.4.3)}$$

where the term $\mathbf{C}_{q_B,q_R}$ is the cross-covariance. It can be neglected since the background and the resonant component are supposed independent. Finally, the equation is written:

$$\mathbf{C}_{q_{BR}} = \mathbf{C}_{q_B} + \mathbf{C}_{q_R}. \quad \text{(III.4.4)}$$

The matrix $\mathbf{C}_{q_{BR}}$ will be compared to the one obtained by integration of the PSD of the displacements.

4.2.1 Background component

The quasi-static response is easily estimated. Indeed, it is simply the resolution of the fundamental equation of motion when there is no internal nor damping terms.

$$\mathbf{x}_B(t) = \mathbf{K}^{-1}\mathbf{f}(t) \quad \text{(III.4.5)}$$

This expression is extended to the covariance matrix:

$$\mathbf{C}_{x_B} = \mathbf{K}^{-1}\mathbf{C}_F\mathbf{K}^{-T}. \quad \text{(III.4.6)}$$

To calculate the covariance of the forces, the covariance of the pressure are computed directly from the experiment samples.

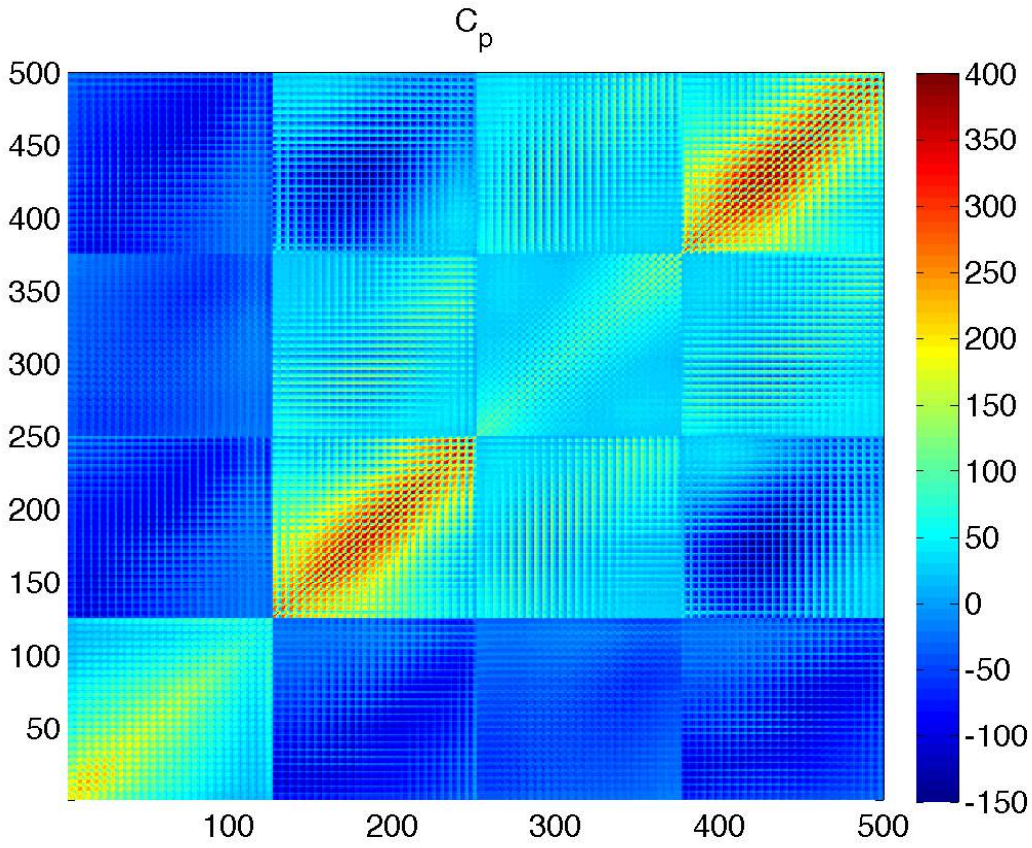

Figure III.4.4: Covariance matrix of the pressure for an angle of attack of 0°.

Then, the covariance of the forces is computed:

$$\mathbf{C}_F = \mathbf{A}\mathbf{C}_p\mathbf{A}^T. \tag{III.4.7}$$

Eventually, as we want to work with the modal displacements, $\mathbf{C}_x$ is projected in the modal basis:

$$\mathbf{C}_{q_B} = \boldsymbol{\phi}^T\mathbf{C}_{x_B}\boldsymbol{\phi}. \tag{III.4.8}$$

It has been shown that seven modes are enough to represent in an accurate way the quasi-static response in the modal basis.

4.2.2 Resonant component

To represent the resonant component of the response, only the PSDs of the pressure at the natural frequencies kept in the modal analysis need to be known. Thus, these matrices can be extracted from the complete PSD matrix of the pressure:

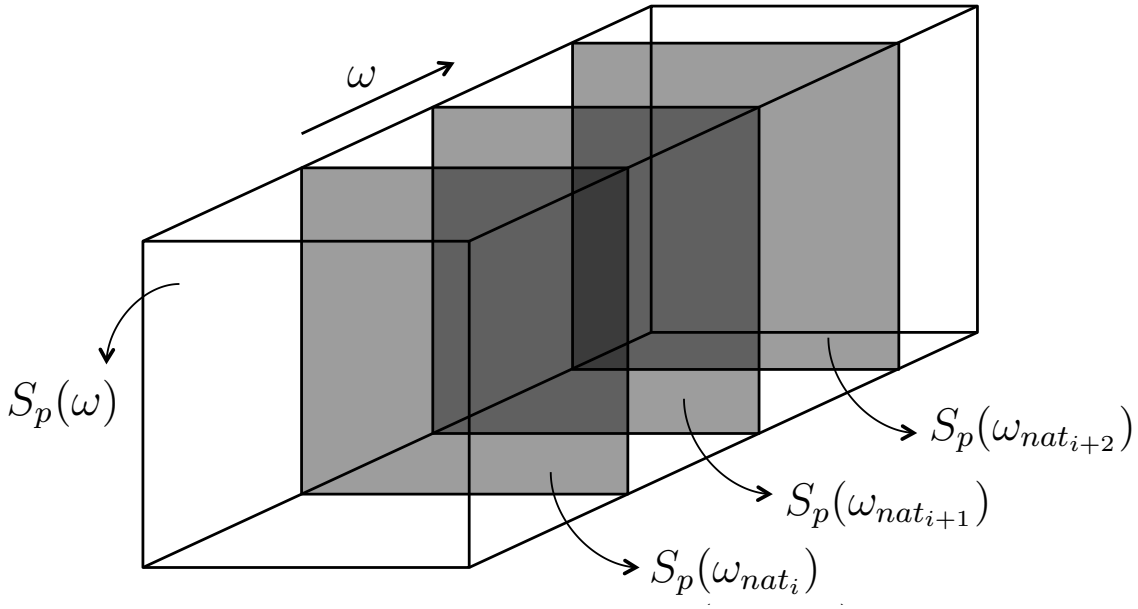

Figure III.4.5: Extraction of the PSD at the natural frequencies.

where $\mathbf{S}_p(\omega_{nat_i})$ is the PSD at the natural frequency i. Finally, we have a matrix with the dimensions $[500 \times 500 \times 7]$ instead of $[500 \times 500 \times 513]$. This leads to a less time and memory consuming implementation.

The PSDs at the natural frequencies are complex but they can be represented in terms of absolute value and argument.

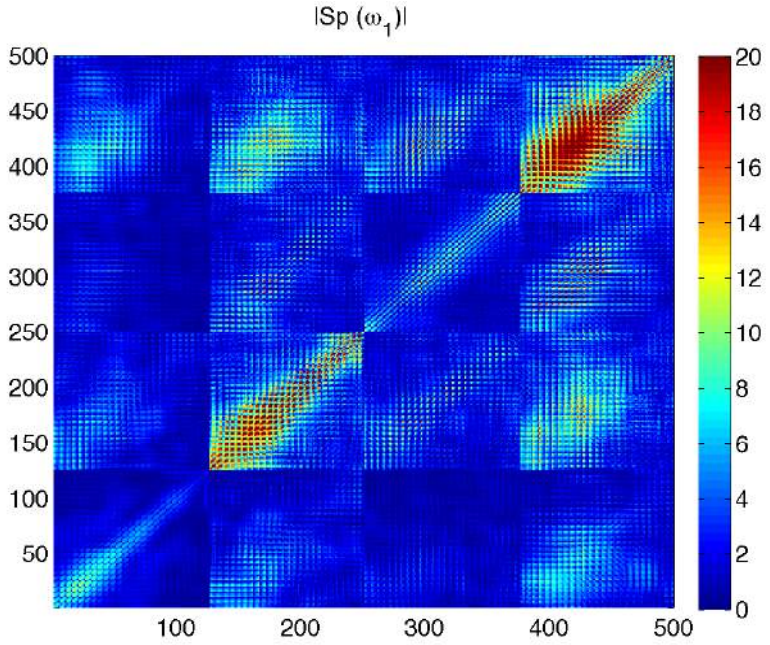

Figure III.4.6: Absolute value of the PSD of the pressure at the first natural frequency for an angle of attack of 0°.

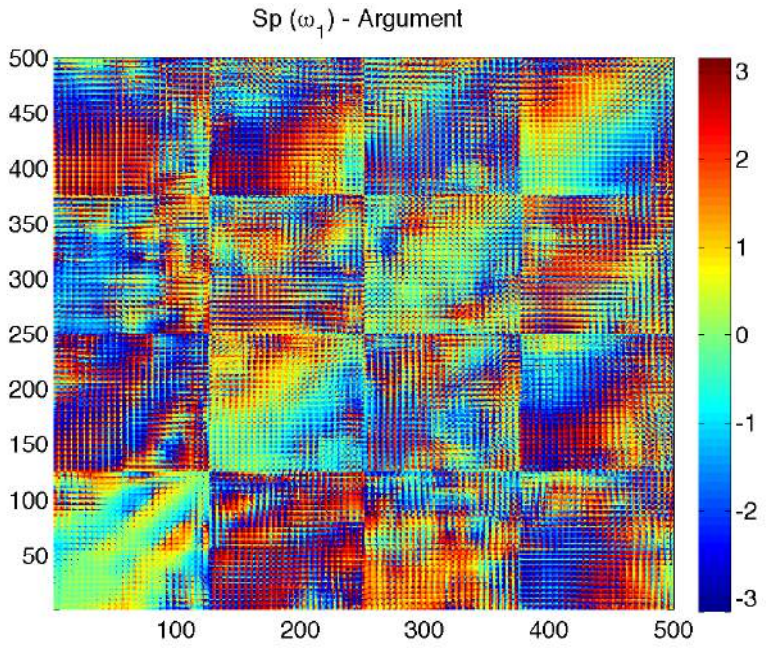

Figure III.4.7: Argument of the PSD of the pressure at the first natural frequency for an angle of attack of 0°.

The matrices above are organised face by face. They will be the starting point of the reconstruction step.

Once these matrices are extracted, the path followed is similar to what has been done previously. First the calculation of the PSD of the forces at these natural frequencies:

$$\mathbf{S}_F(\omega_{nat}) = \mathbf{A}\mathbf{S}_p(\omega_{nat})\mathbf{A}^T. \quad \text{(III.4.9)}$$

And then, the projection of these forces in the modal basis:

$$\mathbf{S}^*_F(\omega_{nat}) = \boldsymbol{\phi}^T\mathbf{S}_F(\omega_{nat})\boldsymbol{\phi}. \quad \text{(III.4.10)}$$

Eventually, the covariance matrix of the modal displacements can be calculated using the equation II.2.41.

4.3 Comparison of the complete stochastic analysis and the background/resonant decomposition.

In order to quantify the error made using the background/resonant decomposition, we compare the standard deviation of the modal displacement and the correlation coefficient matrix. As it was said in the previous chapter, these two are the metrics used to have an estimation of the accuracy of a method.

The standard deviation can be compared for each mode used in the modal decomposition. The other angles of attacks are presented in *Appendix B*.

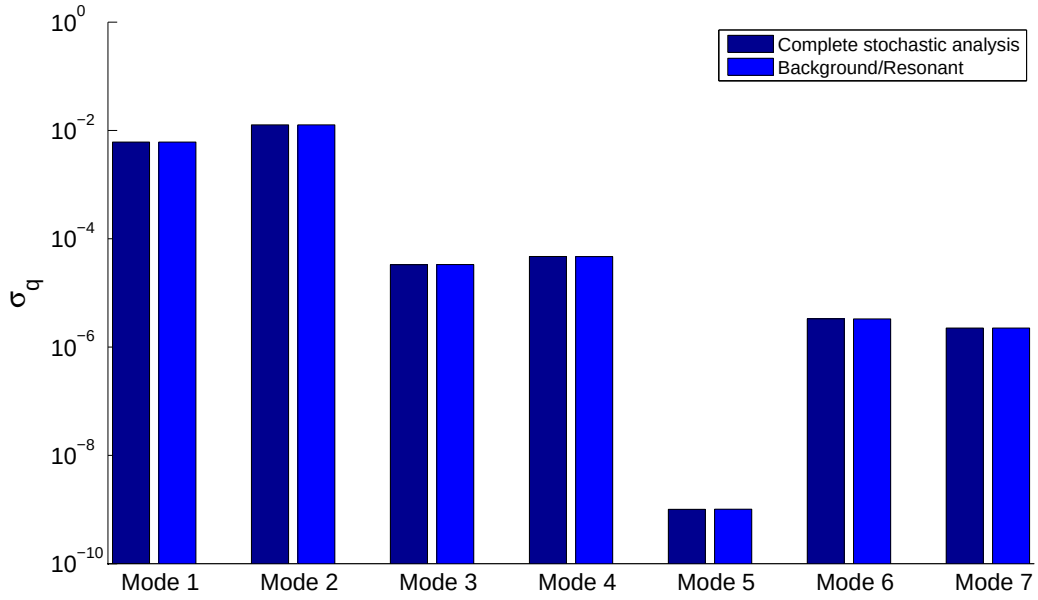

Figure III.4.8: Standard deviation of the modal displacement for the complete analysis and the B/R decomposition for an angle of attack of 0°.

The figure above provides us with a first idea of the accuracy of the B/R decomposition. Indeed, the values are closed to the reference ones. It is possible to quantify the relative error.

	σ_q - Ref $[mm]$	σ_q - B/R $[mm]$	Relative error [%]
Mode 1	**6.102**	**6.084**	**0.297**
Mode 2	**12.677**	**12.634**	**0.335**
Mode 3	3.31810^{-2}	3.33110^{-2}	0.404
Mode 4	4.69710^{-2}	4.68210^{-2}	0.317
Mode 5	1.00910^{-6}	1.01510^{-6}	0.593
Mode 6	3.32910^{-3}	3.30910^{-3}	0.594
Mode 7	2.25210^{-3}	2.24510^{-3}	0.369

Table III.4.1: Comparison of the standard deviation of the modal displacement for an angle of attack of 0° between the reference analysis and the background/resonant decomposition.

The relative error on the standard deviation of the modal displacement made using the background/resonant decomposition is small. The response takes place mainly in the first two modes. For that reason, the relative errors for the other angle of attack are given only for these two modes. The obtained relative errors for the other angles of attack are again really small.

		σ_q - Ref $[mm]$	σ_q - B/R $[mm]$	Relative error [%]
15°	Mode 1	5.090	5.079	0.214
	Mode 2	8.542	8.492	0.591
45°	Mode 1	5.015	5.002	0.260
	Mode 2	5.289	5.287	0.028

Table III.4.2: Comparison of the standard deviation of the modal displacement for different angle of attack between the reference analysis and the background/resonant decomposition.

To definitely validate the method, we compare compare the correlation coefficient matrices in order to quantify the accuracy of the B/R decomposition on the modal correlation.

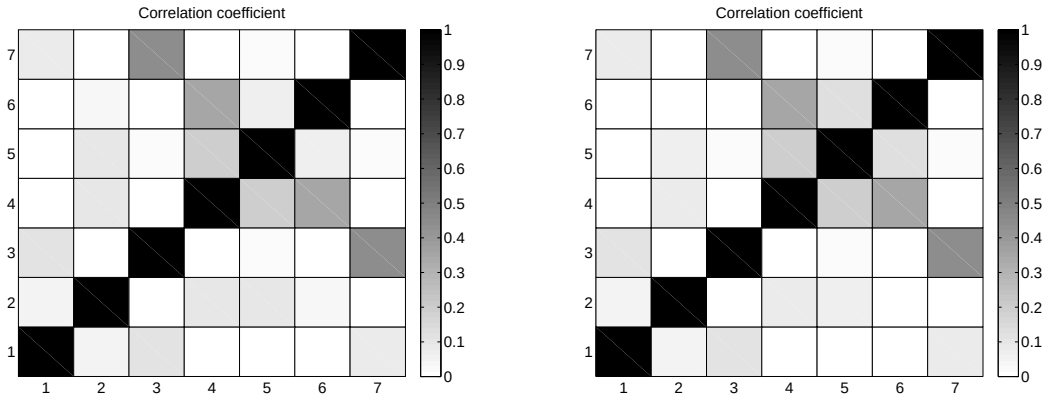

(a) Complete stochastic analysis. (b) Background/Resonant decomposition.

Figure III.4.9: Correlation coefficient of the modal displacement for an angle of attack of 0°.

The obtained correlation coefficient matrix with the background/resonant decomposition is really close to the reference one. As the only meaningful value is the correlation coefficient between the first and the second modes we calculate the error on this value for the different angles of attack.

	ρ_{12} - Ref [−]	ρ_{12} - B/R [−]	Absolute Error [−]
0°	0.051	0.049	0.002
15°	0.177	0.154	0.023
45°	0.056	0.099	0.043

Table III.4.3: Comparison of the modal correlation coefficient of mode 1 and 2 for different angle of attack.

In the case of the correlation, the important is not to reconstruct the value with a small relative error. Indeed, since the standard deviation is accurate, it is only necessary that the absolute difference between the correlation is as small as possible. Moreover as we work with small numbers, it makes more sens to use this definition of the error.

As it can be seen, the difference between the modal correlation in the complete stochastic analysis and the background/resonant decomposition is small. Theses different results validate the use of the background/resonant decomposition.

Part IV

Partial Measurements Analysis

Chapter 1

Multiple setup measurements

The developments made in the first parts of this paper were conducted with all the pressure taps used by *Kikuchi & al.* during their experiments. As discussed in the introduction, most of the time a limited amount of available sensors leads experimenter to use multiple setup measurements.

To illustrate the method developed, we define a reference experimental setup that will be used to explain all the steps from the partial data measured to the reconstructed displacement field. Alternative experimental setups are also defined.

1.1 Reference multiple setups

The main scheme of the multiple setups that are presented is to conduct several experiments with some of the sensors that are fixed and some of them that are moving across the structure.

The reference experimental multiple setup consists of 4 configurations where 104 taps are fixed and 99 taps are moving. The fixed taps are placed in two columns, one row on two on each face. The moving taps will fill each face one by one so that 4 configurations are obtained.

The figure below illustrates the first configuration.

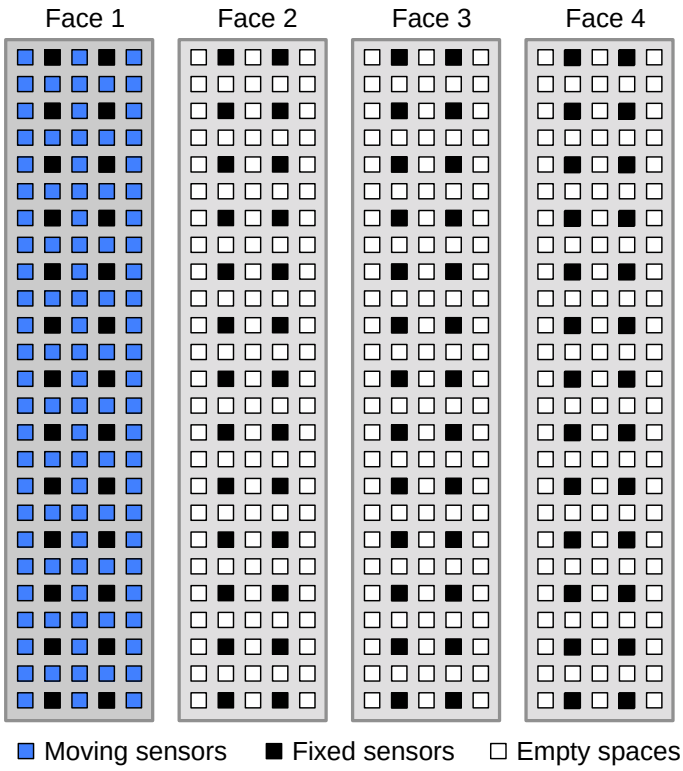

Figure IV.1.1: First configuration of the reference experimental setups

The three other configurations consist simply in moving the blue taps on the three other faces. It is worth noticing that we chose to put the same number of fixed taps on each face. Indeed, as we are looking at different angles of attacks, we need to extract a maximum of informations for each wind incidence.

Eventually, instead of getting from the experiments the full covariance and PSD matrices of the pressure, we have a lack of information on the relation between some taps since they are not measured synchronously. To illustrate this we look at the covariance matrix of the pressure we got from complete measurements on figure III.4.4.

The missing information can be removed to get the matrix we have after the experiment with a limited number of sensors (figure IV.1.2). The blank spaces are the unknown data that we need to reconstruct.

The same process is applied on the PSD of the pressure at the natural frequencies. These matrices will be the new starting point of the analysis so that a reconstruction step is needed before the straight application of the background/resonant decomposition described above.

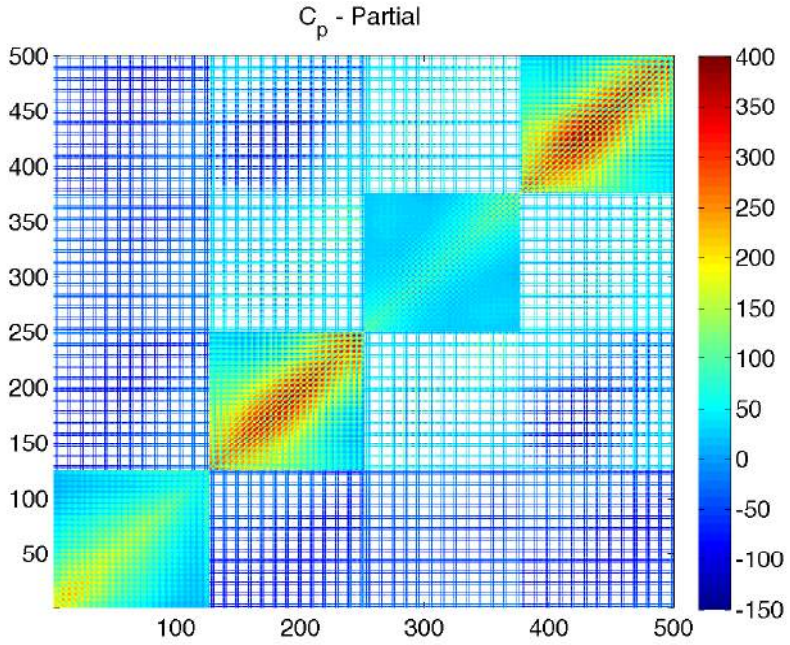

Figure IV.1.2: Covariance matrix of the pressure from the reference measurements setup

1.2 Alternative setups

It exists an huge number of multiple setup configurations. In order to have different comparison points, two alternative setups are presented.

Alternative setup 1

The first alternative setup consists in 100 fixed taps and 100 moving taps. The fixed ones, are placed as one column by face and 6 row that follow all the circumference of the building. The moving taps will fill each face like what it was done in the reference multiple setup.

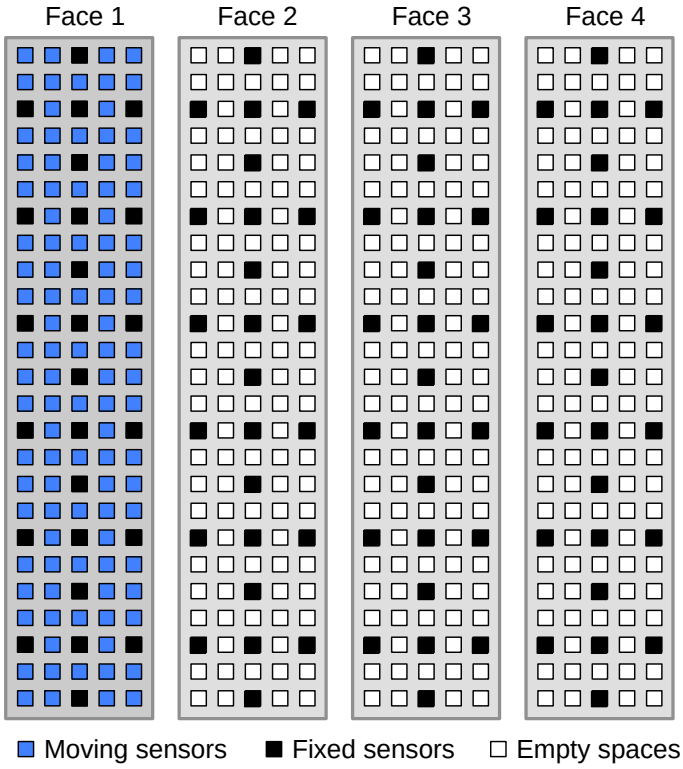

Figure IV.1.3: First configuration of the alternative setups

This configuration as the advantage that we also measure information about the correlation across each face at a same level.

Alternative setup 2

In order to increase the importance of the measurement of this correlation between the different faces, it is possible to change the way of using the moving sensors.

In this second alternative setup, the 100 fixed sensors stay the same. Concerning the moving taps, they are placed on each face but only on a certain height of the building. Then, they will go down in order to cover all the building with the different configurations. As an example, with 128 sensors the entire building is covered with 3 setups.

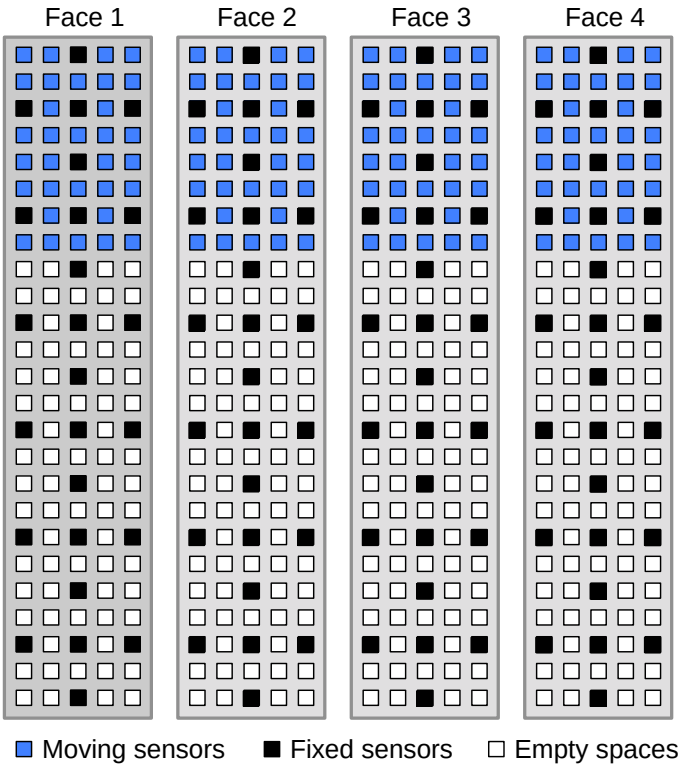

Figure IV.1.4: First configuration of the second alternative setups

Eventually, it possible to summarise the properties of the different setups.

	Reference (SVD 1)	Alternative 1 (SVD 2)	Alternative 2 (SVD 3)
Setups	**4**	**4**	**3**
Fixed sensors	104	100	100
Moving sensors	99	100	128
Total	**203**	**200**	**228**

Table IV.1.1: Characteristics of the different multiple setups measurement studied.

As it can be seen, the two first multiple setups scheme are similar in terms of sensors and setups. The last one need a bit more sensors but only 3 setups. The three schemes are called *SVD 1*, *SVD 2* and *SVD 3*.

Chapter 2

Reconstruction of incomplete measurements

The experiment conducted with a limited number of sensors and different configurations gives us partial information on the statistical properties of the pressure. It means that we need to fill the gaps in our covariance and PSD matrices in order to design properly our structure.

There are different ways to guess the missing information such as filling with random value [3]. However, this approach is limited because the positive definite condition of the matrices we want to approximate need to be fulfilled. Thus, it is important to think at more appropriate method to apply.

One of them is to apply the Singular Value Decomposition on the know part of the matrix in order to extract the principle directions of it and to use them to reconstruct a complete matrix with the same properties.

2.1 Application of the Singular Value Decomposition

The reconstruction using the SVD is applied on the partial matrices. We work with the covariance matrix of the pressure to illustrate the process but the method is similar for the PSD of the pressure at each natural frequency.

The rectangular matrix in the red box, called $\hat{\mathbf{C}}_p$, is known (figure IV.2.1). We apply the SVD on it.

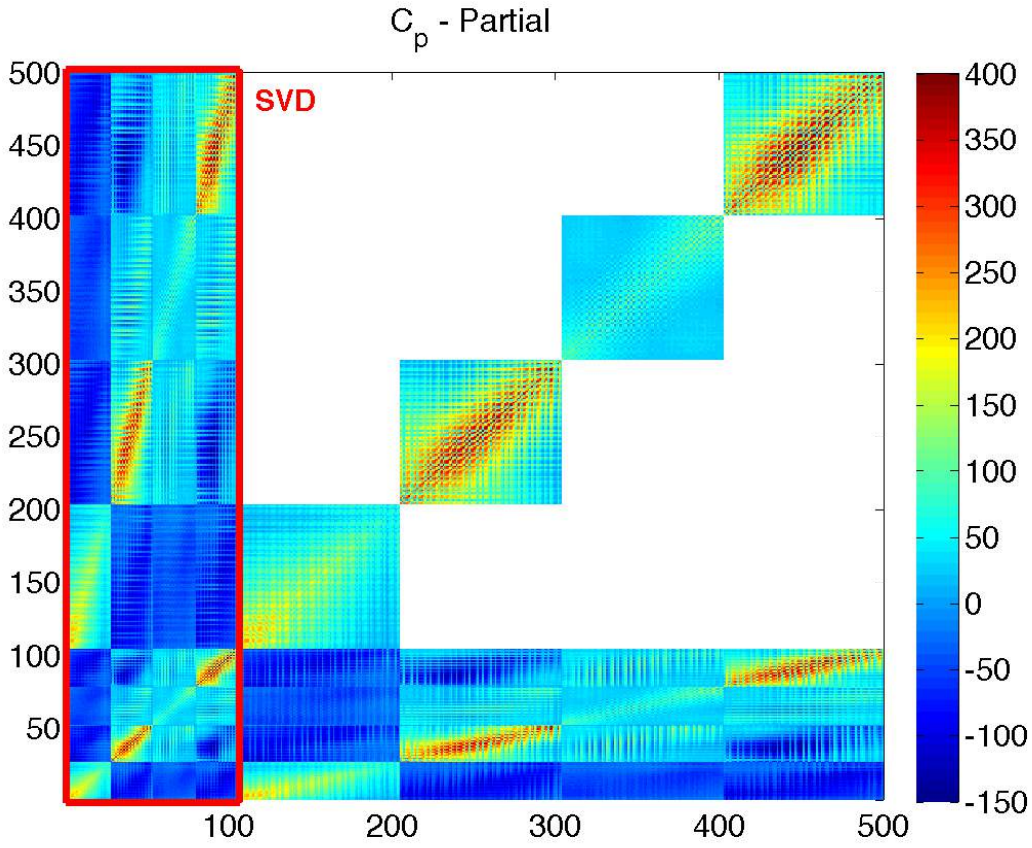

Figure IV.2.1: Extraction of a rectangular matrix from the covariance of the pressure to apply the SVD.

The SVD is written as described in the theoretical part:

$$\underbrace{\hat{\mathbf{C}}_p}_{500\times104} = \underbrace{\mathbf{U}}_{500\times500}\ \underbrace{\mathbf{\Sigma}}_{500\times104}\ \underbrace{\overline{\mathbf{V}}^T}_{104\times104} \tag{IV.2.1}$$

It is possible to extract the singular values and vectors from the $\mathbf{U}$ and $\mathbf{\Sigma}$ matrices in order to generate a matrix with the same first directions:

$$\underbrace{\tilde{\mathbf{C}}_p}_{500\times500} = \underbrace{\hat{\mathbf{U}}}_{500\times104}\ \underbrace{\hat{\mathbf{\Sigma}}}_{104\times104}\ \underbrace{\hat{\mathbf{U}}^T}_{104\times500} \tag{IV.2.2}$$

where $\hat{\mathbf{\Sigma}}$ is a diagonal matrix with the singular values on it, $\hat{\mathbf{U}}$ a rectangular matrix containing the singular vectors on its columns and $\tilde{\mathbf{C}}_p$ the approximation of the real covariance matrix of the pressure.

2.2 Scaling of the reconstructed matrix

One of the main issues using the SVD reconstruction is that we overwrite values we know from the measurements. Especially the squares on the diagonal on the figure IV.2.1.

The simplest way to avoid this problem would be to replace only the blank spaces of the partial matrix with corresponding values obtained with the SVD reconstruction. However, the positive definite condition would no longer be fulfilled, which means that this first option is not applicable.

The other solution would be to scale the matrices from SVD reconstruction in order to get a better approximation of the value measured in the multiple setups. The scaling consists in pre and post multiplying the reconstructed matrix, $\tilde{\mathbf{C}}_p$, by a scaling matrix, $\mathbf{D}$ in such way to keep the symmetry:

$$\tilde{\tilde{\mathbf{C}}}_p = \mathbf{D}^{0.5}\tilde{\mathbf{C}}_p\mathbf{D}^{T0.5} \tag{IV.2.3}$$

where the values in the scaling matrix need to be defined on criteria that will be discussed below in such way that:

$$\tilde{\tilde{\mathbf{C}}}_p \approx \mathbf{C}_p. \tag{IV.2.4}$$

2.2.1 Diagonal elements

Two different ways of scaling are presented. The first option consists in scaling the matrix from SVD reconstruction in order to obtain the same diagonal as the partial measurements matrices. In the case of the covariance matrix, it means having a perfect estimation of the variances.

The scaling matrix will be a diagonal matrix with the values on its diagonal defined as:

$$D_i = \frac{C_{p_i}}{\tilde{C}_{p_i}}. \tag{IV.2.5}$$

With this approach, the scaling matrix is easy to define because all the values needed are known. Eventually we obtain covariance matrix of the pressure presented on figure IV.2.2.

This simple but accurate approach is used to calculate the error made using the SVD reconstruction.

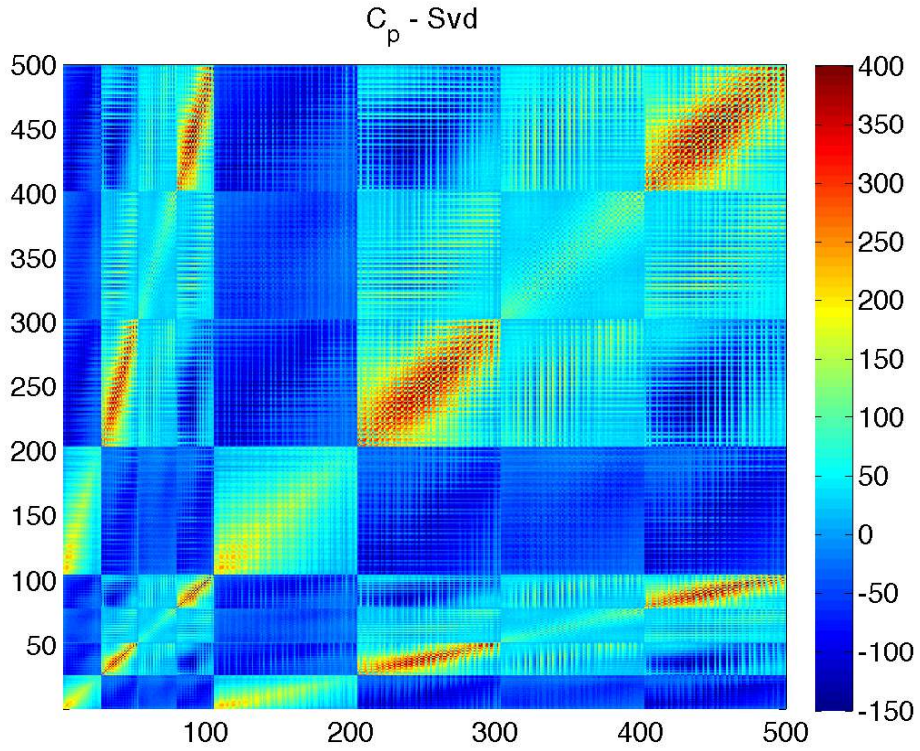

(a) Organised fixed taps - moving taps.

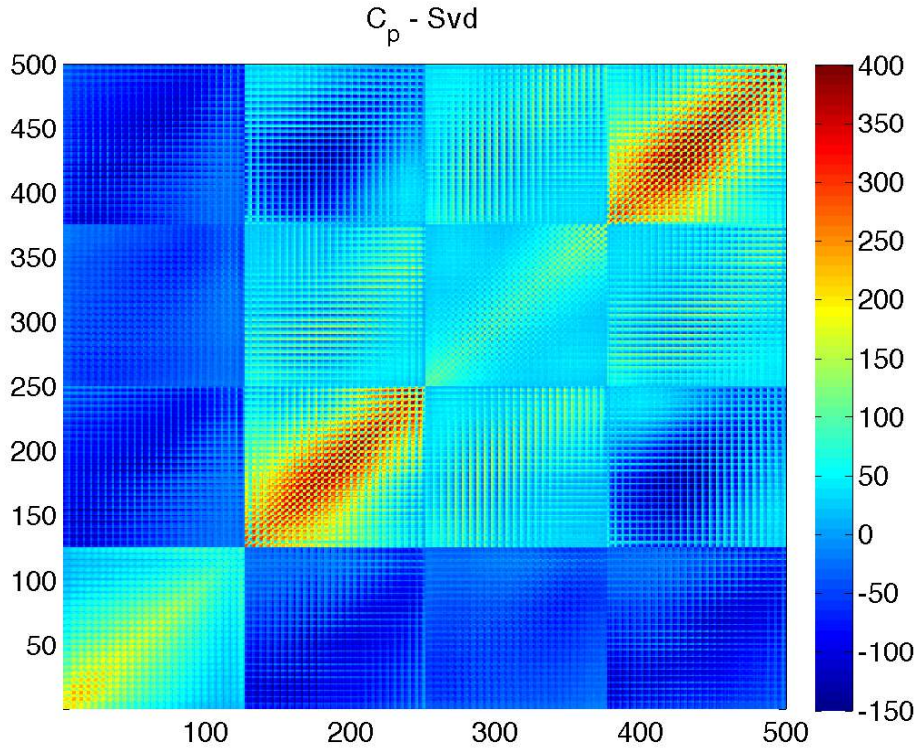

(b) Organised face by face.

Figure IV.2.2: Covariance matrix of the pressure from the reference measurements setup

2.2.2 Full measurements data

The scaling described above has the advantage to be easy to implement. Unfortunately, we still overwrite a lot of values known from the measurements. To avoid that, an option would be to use a different scaling matrix in order to get a reconstructed matrix in which all the values known from the measurements would be as close as possible from the real ones.

The main idea is to use a mathematical criteria to express the "as close as possible" condition. One possibility is to use the absolute difference between the scaled and the measured values and to minimise its norm:

$$\rightarrow min(||\mathbf{c}_p - \tilde{\tilde{\mathbf{c}}}_p||) \tag{IV.2.6}$$

where $\mathbf{c}_p$ is a vector containing all the values measured and $\tilde{\tilde{\mathbf{c}}}_p$ is a vector containing the corresponding values obtained with the SVD reconstruction and scaled with a scaling matrix $\mathbf{D}$.

As the values measured and the values from the SVD reconstruction are fixed, the only variables of this optimisation problem are in the scaling matrix. This matrix must be $[500 \times 500]$ which means that we have at our disposal 250000 degrees of freedom to find the minimum.

Using a matrix full of variables is numerically problematic reading to the time. Alternative shape can be defined such as a diagonal, a band or a triangular matrix.

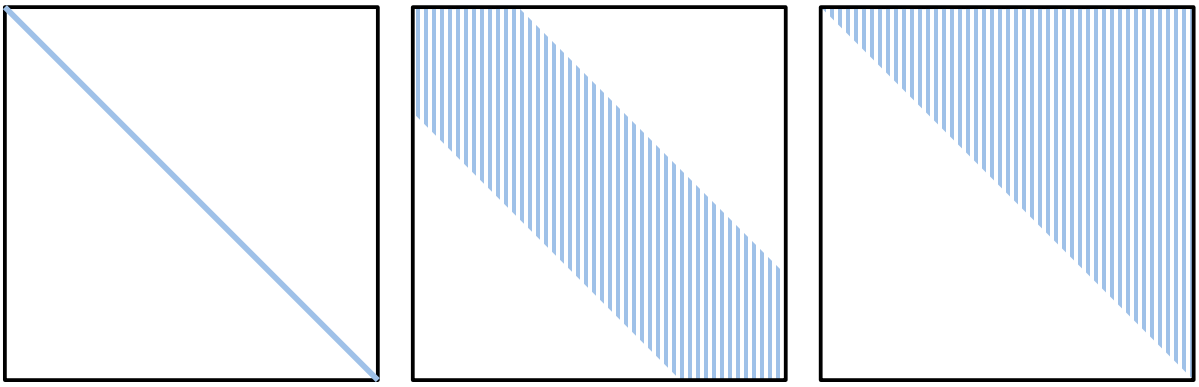

Figure IV.2.3: Alternative shapes for the scaling matrix.

The blank spaces are filled with zero and the hatched spaces are the kept variables.

This approach has been implemented for some extracted parts of the $\mathbf{C}_p$ matrix. Even if the results are promising, the calculation time is already important, which means that it is still not possible to use it on the full $\mathbf{C}_p$ matrix.

To reduce the complexity on this optimisation, a solution could be to find an analytical expression of the problem in order to solve it directly.

Chapter 3

Results

The last step of our work is to analyse the results and to quantify their accuracy. For that, we use the metric defined above,that is to say the relative error on the standard deviation and the absolute error on the correlation of the modal displacements. These quantities are calculated with the different multiple setups defined above and compared to the reference results from the complete stochastic analysis with all the sensors.

3.1 Standard deviation

The first comparison point chosen is the standard deviation of the modal displacements. As it was shown previously, the response takes place in the two first modes for each wind incidence. Thus, only the standard deviation in these modes is compared.

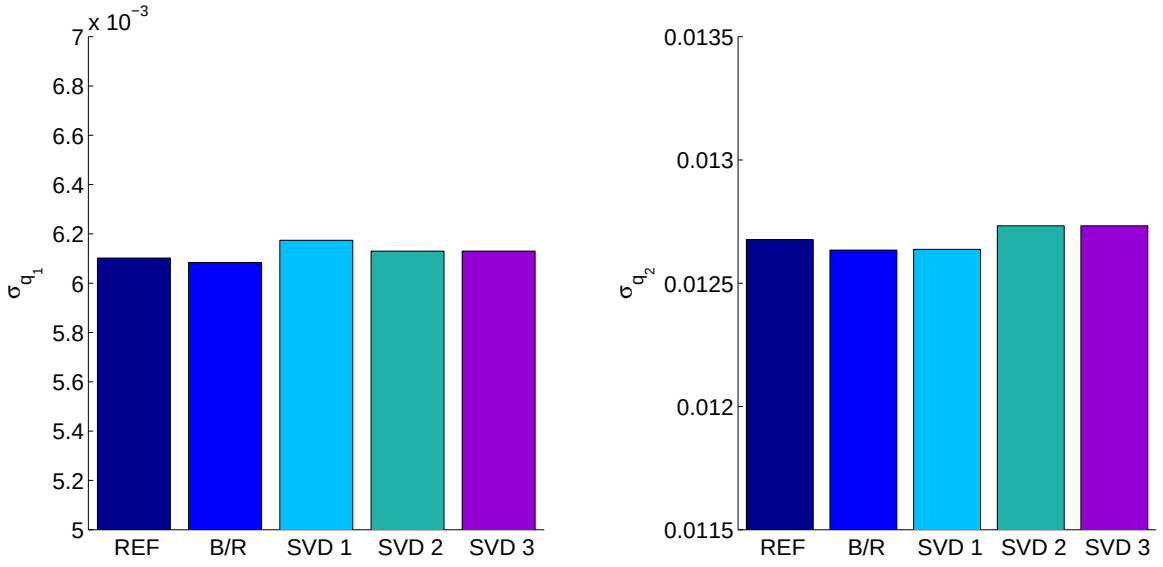

Figure IV.3.1: Standard deviation of the modal displacements in the first and the second modes with an wind incidence of 0°.

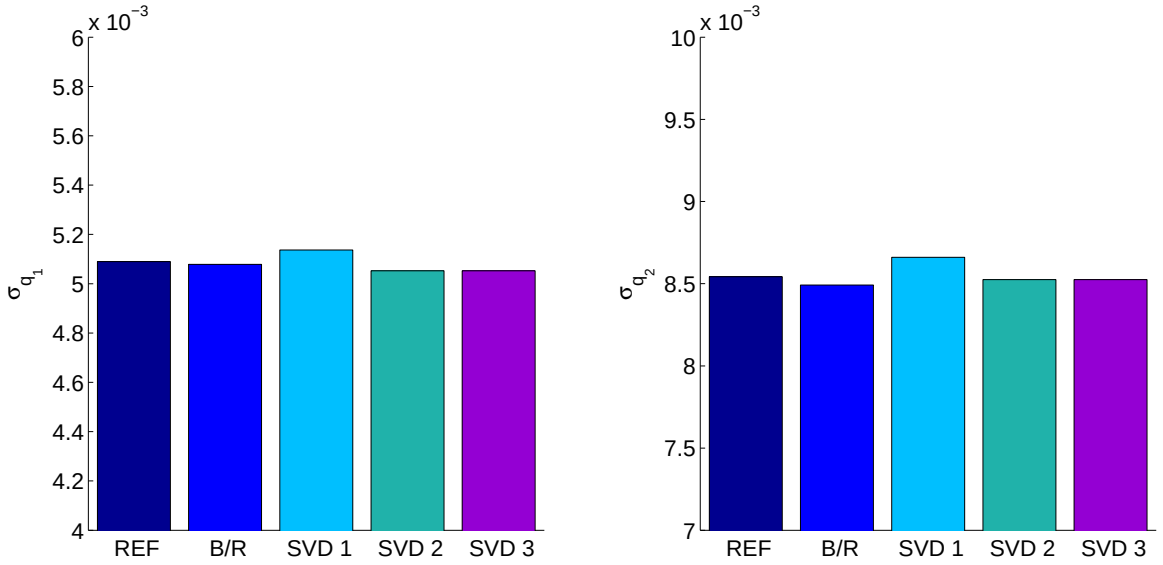

Figure IV.3.2: Standard deviation of the modal displacements in the first and the second modes with an wind incidence of 15°.

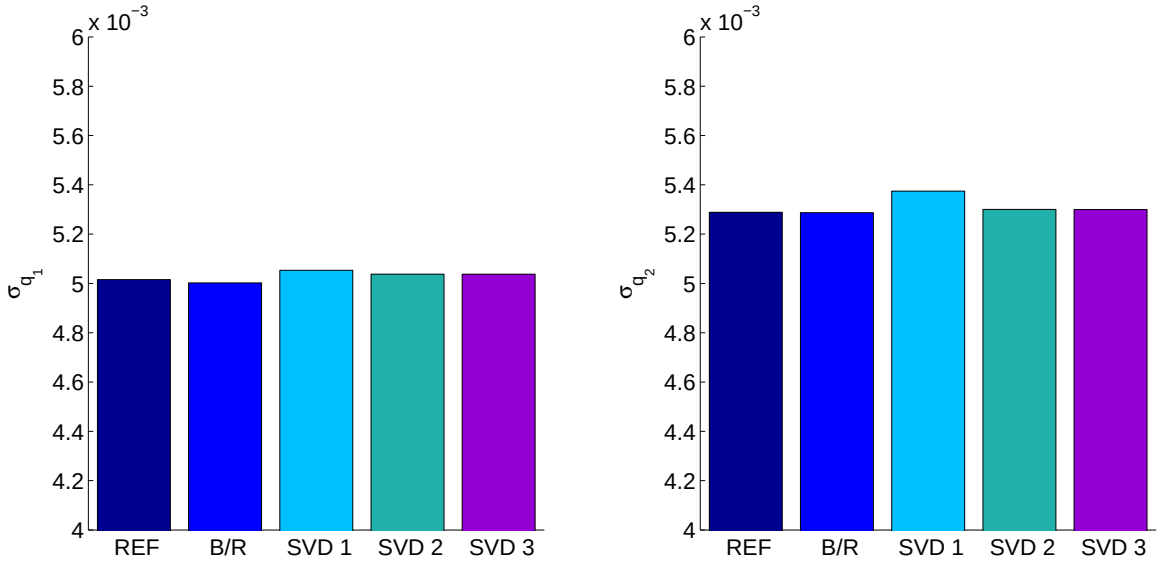

Figure IV.3.3: Standard deviation of the modal displacements in the first and the second modes with an wind incidence of 45°.

The figures above represent the standard deviations calculated with the different methods. The general observation is that all the results are close to the reference ones. It is difficult to define the best approach only with these bar graphs. In order to have a better idea of the accuracy of the reconstruction, it is interesting to calculate the relative error between the multiple setups and the complete analysis.

	0°		15°		45°	
	Mode 1	Mode 2	Mode 1	Mode 2	Mode 1	Mode 2
σ_q - Reference $[mm]$	6.102	12.677	5.090	8.543	5.015	5.289
σ_q - Svd 1 $[mm]$	6.174	12.637	5.137	8.660	5.053	5.375
Relative error [%]	**1.18**	**0.31**	**0.93**	**1.38**	**0.76**	**1.63**
σ_q - Svd 2 $[mm]$	6.130	12.733	5.052	8.525	5.038	5.300
Relative error [%]	**0.46**	**0.44**	**0.73**	**0.21**	**0.44**	**0.22**
σ_q - Svd 3 $[mm]$	6.130	12.733	5.052	8.525	5.038	5.300
Relative error[%]	**0.46**	**0.44**	**0.73**	**0.21**	**0.44**	**0.22**

Table IV.3.1: Comparison of the standard deviation of the modal displacement for different angle of attack.

The obtained relative errors on the standard deviation are smalls. The general observation that can be made from this table is that the two alternative setups (Svd 2 & Svd 3) are as accurate as each other but are both more accurate than the Svd 1.

This leads us to a first outcome. The fixed sensors used in both Svd 2 and Svd 3 are the same, the setups differ only by the moving taps and their accuracy is similar. On the other hand, the moving sensors in Svd 1 and Svd 2 are exactly the same. The difference between them is the reference fixed sensors used and the accuracy is better when using Svd 2.

This would mean that the choice of the moving setups has less importance. The most important feature of the multiple setup measurements would be to chose strategic location to place the fixed sensors.

3.2 Modal correlation

The second metric used is the absolute error on the modal correlation. As it was done when studying the background/resonant decomposition, only the correlation between the two modes in which the response takes place will be compared to the reference one.

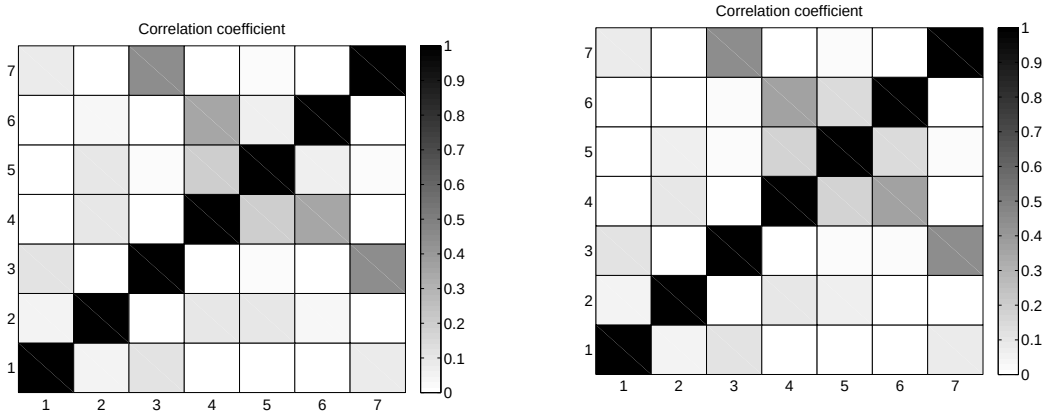

(a) Complete stochastic analysis.

(b) Reconstructed correlation coefficient matrix (Svd 1).

Figure IV.3.4: Correlation coefficient of the modal displacement for an angle of attack of 0°.

	0°	15°	45°
ρ_{12} - Reference [−]	0.049	0.177	0.056
ρ_{12} - Svd 1 [−]	0.056	0.161	0.114
Absolute error [-]	**0.007**	**0.016**	**0.058**
ρ_{12} - Svd 2 [−]	0.057	0.125	0.099
Absolute error [-]	**0.008**	**0.052**	**0.043**
ρ_{12} - Svd 3 [−]	0.058	0.125	0.099
Absolute error[-]	**0.009**	**0.052**	**0.043**

Table IV.3.2: Comparison of the correlation coefficients of the modal displacement for different angle of attack .

The absolute errors presented in the table above are again really smalls. The maximum difference between the reference correlation and a reconstructed one is 0.058. The only relevant observation that can be made is that the reconstructed coefficients of Svd 2 and Svd 3 are the same, which shows the implication of the fixed sensors. It is not possible to draw a general conclusion on the most accurate setup to reconstruct the correlation coefficients.

Theses results are encouraging and foreshadow a robust and accurate method. However, it is important be careful. Indeed, such small errors on the modal correlation and the standard deviation need to be validated by testing the method on other models in order to have several comparison points.

Part V

Conclusion

Conclusion

This master's thesis aimed to develop a method to reconstruct wind pressure field from incomplete measurements. Using multiple setup measurements in a wind tunnel experiment provides only a partial information on the correlation and the coherence between the different places of a structure.

This problem is formulated in a statistical framework using a stochastic approach. The background/resonant decomposition is applied. The quasi-static part is represented by the correlation matrix of the pressure at different locations of the structure and the resonant part by the PSD matrix of these pressures. The partial measurements lead to missing information in these matrices.

We have proposed the use of a singular value decomposition method for the reconstruction of the missing data. This non parametric method is shown to be a robust interpolation tools. It allows to extract the main directions of a set of data, in our case the measured correlation and coherence. These principle directions are used to generate a complete set of data with the same properties.

This method works perfectly when the information extracted from the partial measurements represents the main direction of the complete data. In other words, the key feature of this method lies in the choice of strategic places for the reference sensors used in the multiple setup measurements.

The concept has been illustrated with the pressure field over a rectangular prism. We show that with 4 setups and 200 sensors, we are able to reproduce a response that is close to the one obtained with 500 sensors. The maximum relative error on the standard deviation of the modal displacement is 0.73 %. We also show that an alternative scheme with 3 setups and 238 sensors provides the same results.

These results are encouraging and highlight the accuracy of the method if an appropriate multiple setup measurements experiment is conducted. Moreover the accuracy remains similar for different wind angles of attack.

Although we have focused on a simple rectangular prism, the concept may be extended to more complex structures. Indeed, as the method developed is non parametric, the same scheme of fixed and moving sensors could be applied on other civil works such as stadium roof or bridges. And eventually, beside the interest in the civil engineering field, this method could also find its place in the other engineer fields such as mechanics and aeronautic.

List of Figures

List of Tables

Bibliography

[1] SOLARI G., CARASSALE L., TUBINO F., *Proper orthogonal decomposition in wind engineering. Part 1 : A state-of-the-art and some prospects*, Wind and Structures. Vol 10, No. 2 (2007).

[2] KIKUCHI H., TAMURA Y., UEDA H., HIBI K., *Dynamic wind pressures acting on a tall building model - proper orthogonal decomposition*, Journal of Wind Engineering and Industrial Aerodynamics 69-71 (1997).

[3] BELLINA L., *Reconstruction of the correlation matrix of wind pressures from multiple setup measurements*, 2015.

[4] DENOEL V., *Analyse de structures soumises au vent turbulent : de l'approche stochastique fréquentielle au dynamique transitoire non linéaire*, 2003.

[5] DENOEL V., *Estimation of modal correlation coefficients from background and resonant responses*, Structural Engineering and Mechanics, Vol. 32, No. 6 (2009).

[6] DENOEL V., *Analyse dynamique des structures du génie civil*, 27 octobre 2010.

[7] MICHAEL A., *Deterministic model.*, A Dictionary of Ecology, 2004.

[8] CHANG K. C., *Determination of the Strouhal number based on the aerodynamic behavior of rectangular cylinders*, Wind and Structures, Vol. 3, No. 3 (2000).

[9] DUTTA S., PANIGRAHI P. K., MURALIDHAR K., *Experimental Investigation of Flow Past a Square Cylinder at an Angle of Incidence*, Journal of engineering mechanics (2008).

Appendix A

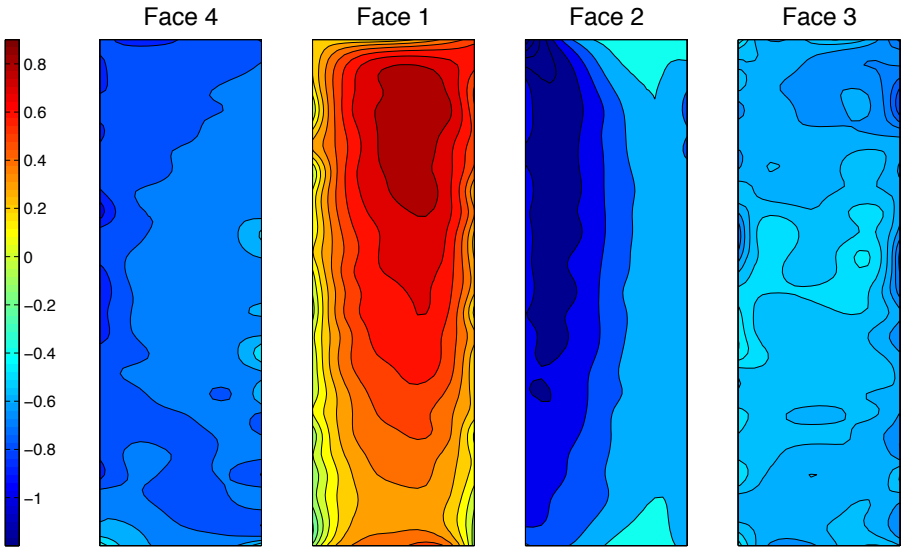

Figure A.1: Mean pressure on the four faces for an angle of attack of 15°.

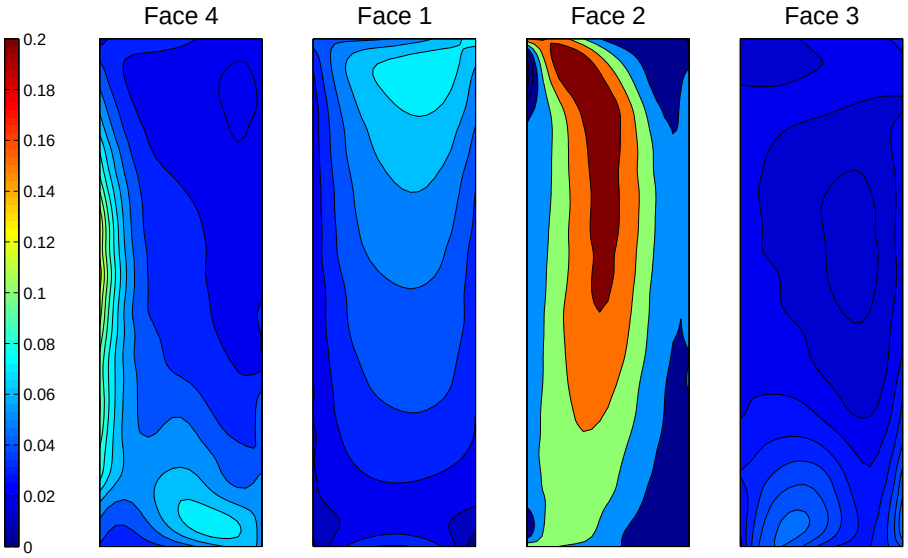

Figure A.2: Variance of the pressure on the four faces for an angle of attack of 15°.

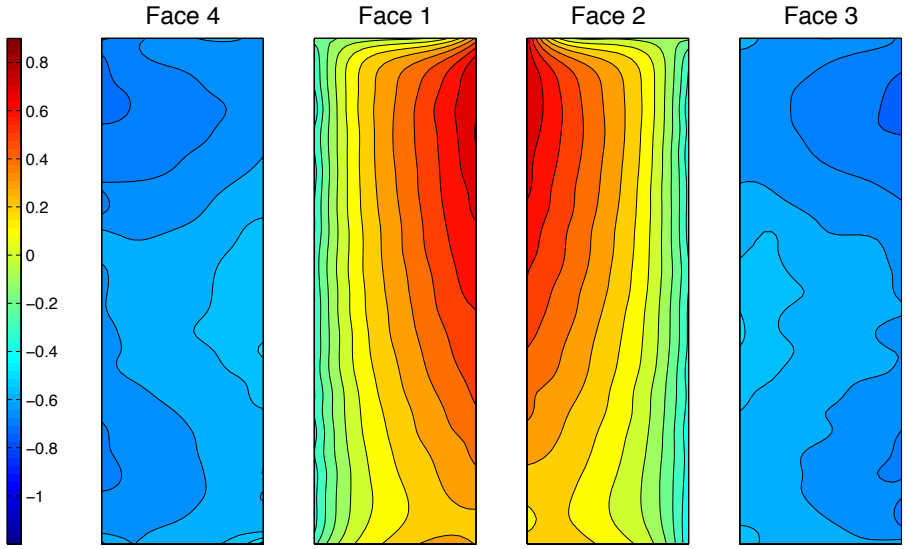

Figure A.3: Mean pressure on the four faces for an angle of attack of 45°.

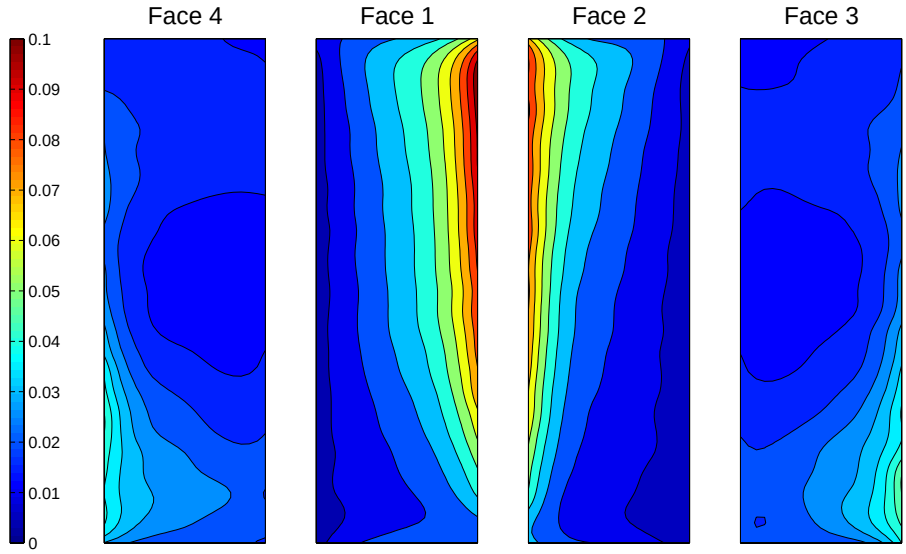

Figure A.4: Variance of the pressure on the four faces for an angle of attack of 45°.

Appendix B

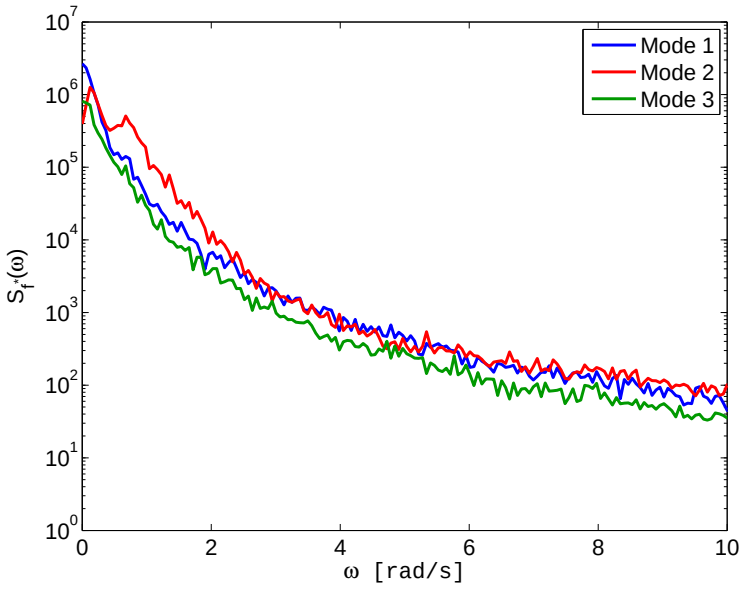

Figure B.1: PSD of the modal forces in the first three modes for an angle of attack of 15°

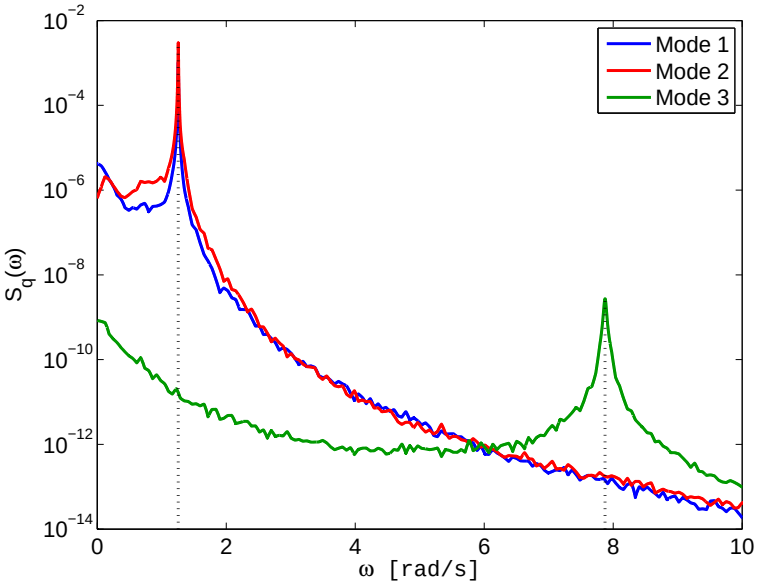

Figure B.2: PSD of the modal displacement in the first three modes for an angle of attack of 15°

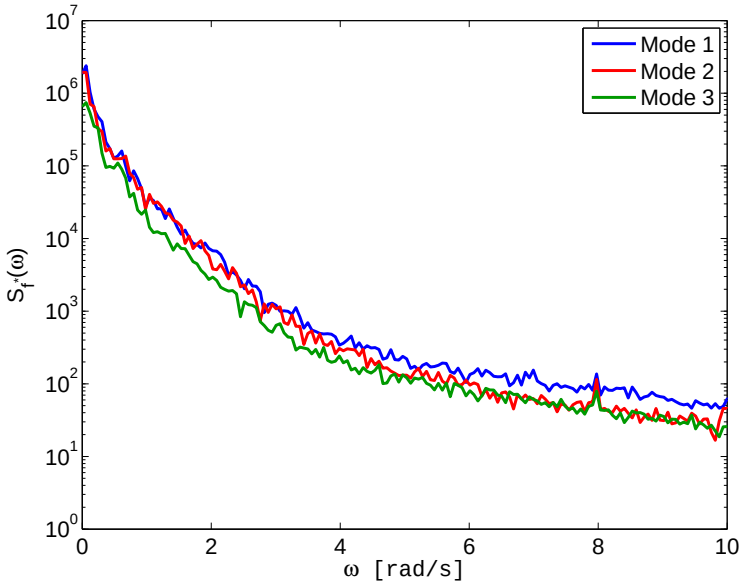

Figure B.3: PSD of the modal forces in the first three modes for an angle of attack of 45°

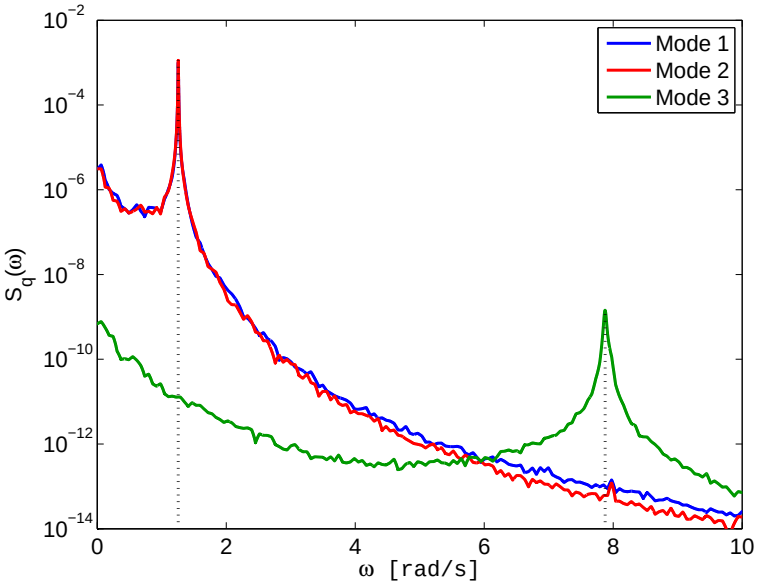

Figure B.4: PSD of the modal displacement in the first three modes for an angle of attack of 45°

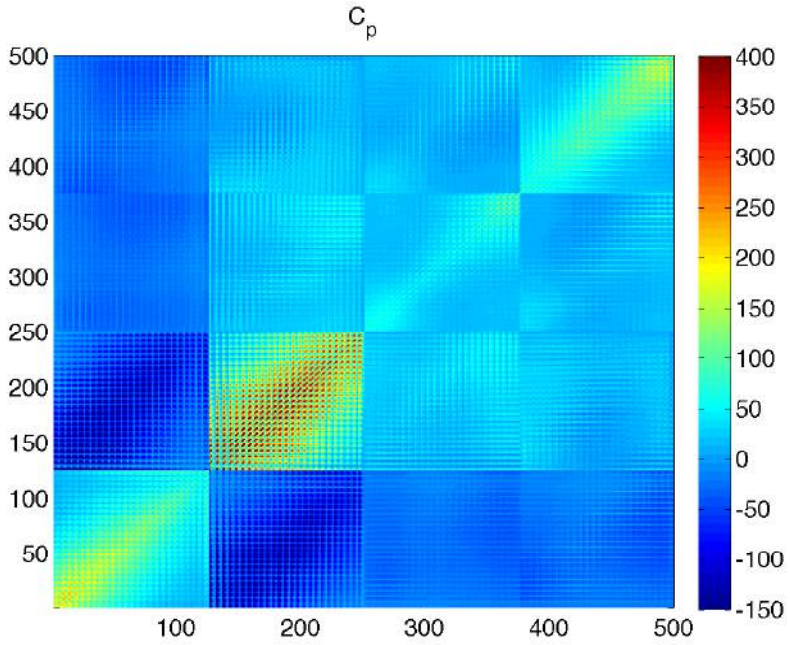

Figure B.5: Covariance matrix of the pressure for an angle of attack of 15°.

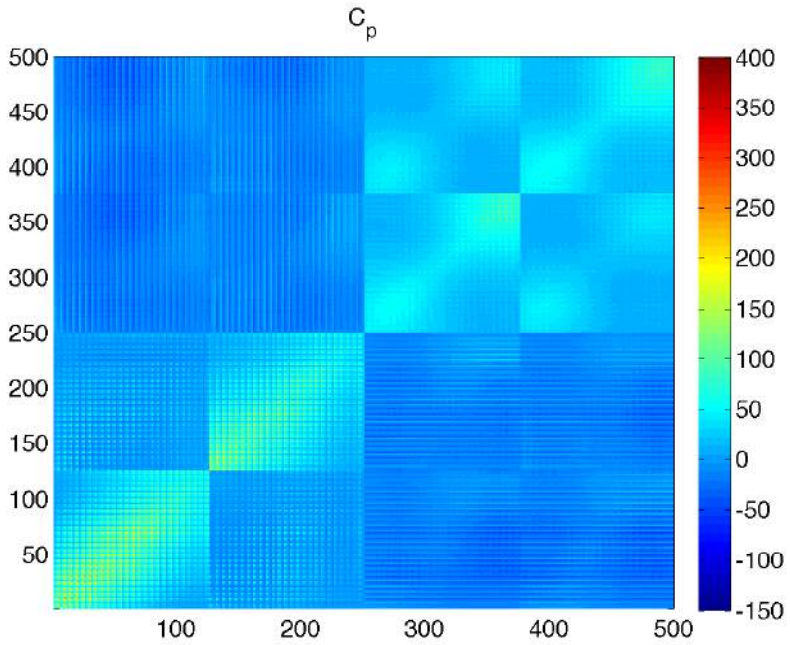

Figure B.6: Covariance matrix of the pressure for an angle of attack of 45°.

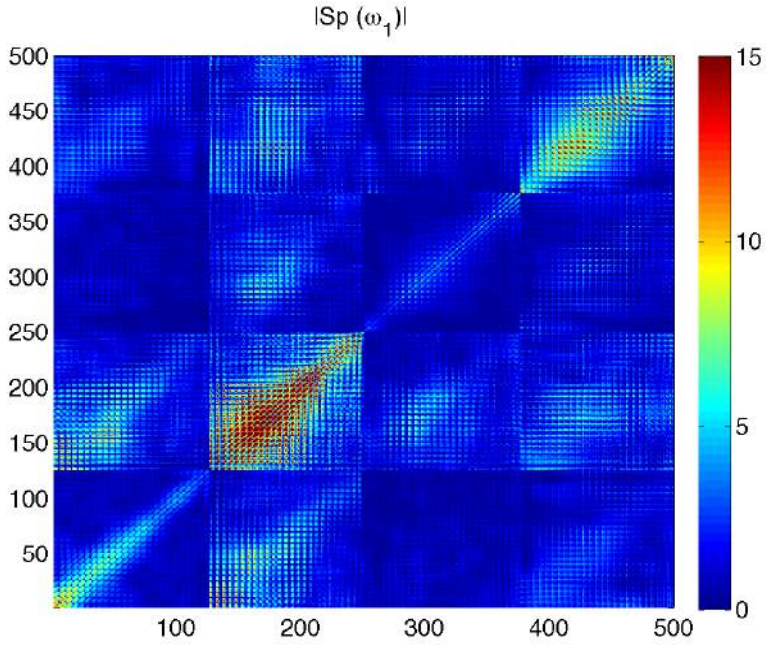

Figure B.7: Absolute value of the PSD of the pressure at the first natural frequency for an angle of attack of 15°.

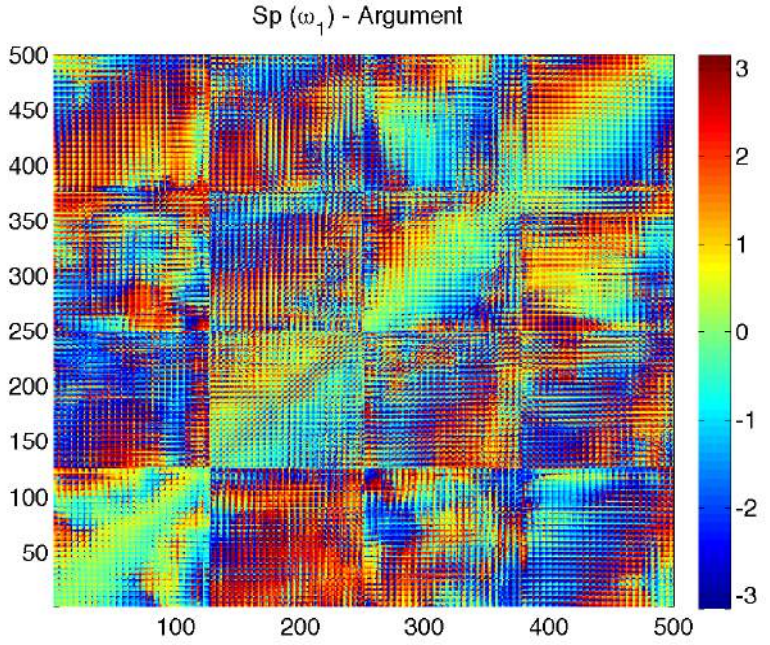

Figure B.8: Argument of the PSD of the pressure at the first natural frequency for an angle of attack of 15°.

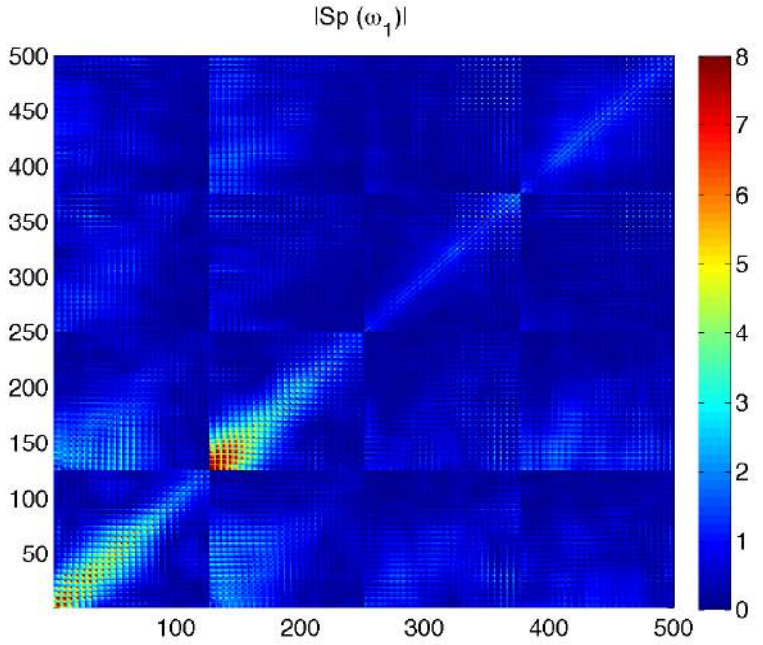

Figure B.9: Absolute value of the PSD of the pressure at the first natural frequency for an angle of attack of 45°.

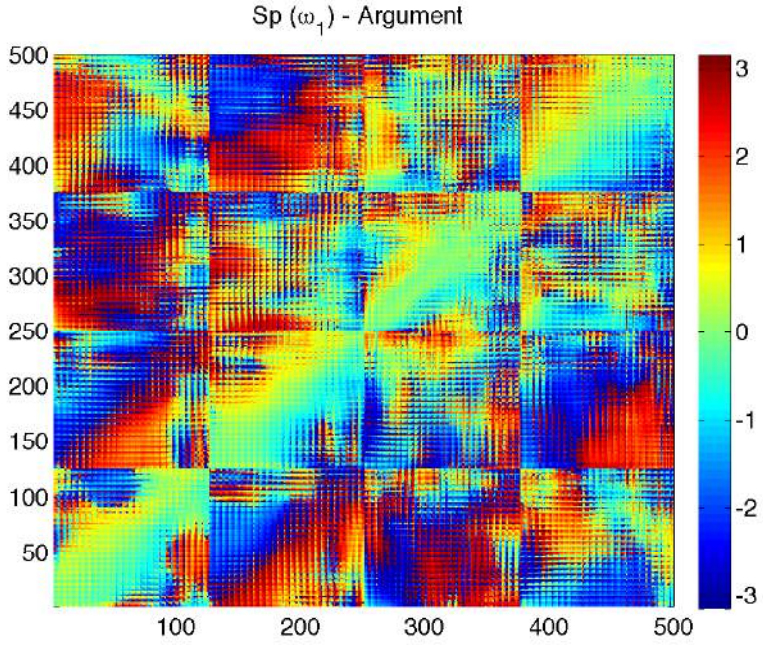

Figure B.10: Argument of the PSD of the pressure at the first natural frequency for an angle of attack of 45°.

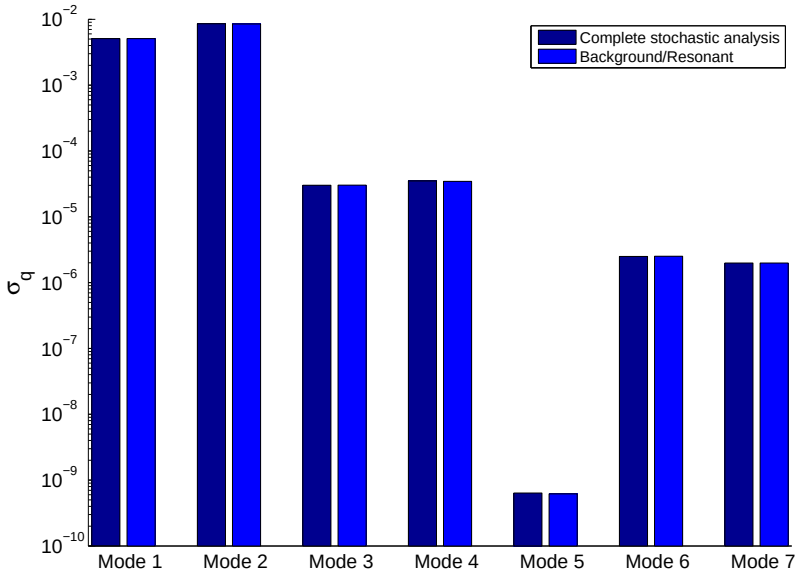

Figure B.11: Standard deviation of the modal displacement for the complete analysis and the B/R decomposition for an angle of attack of 15°.

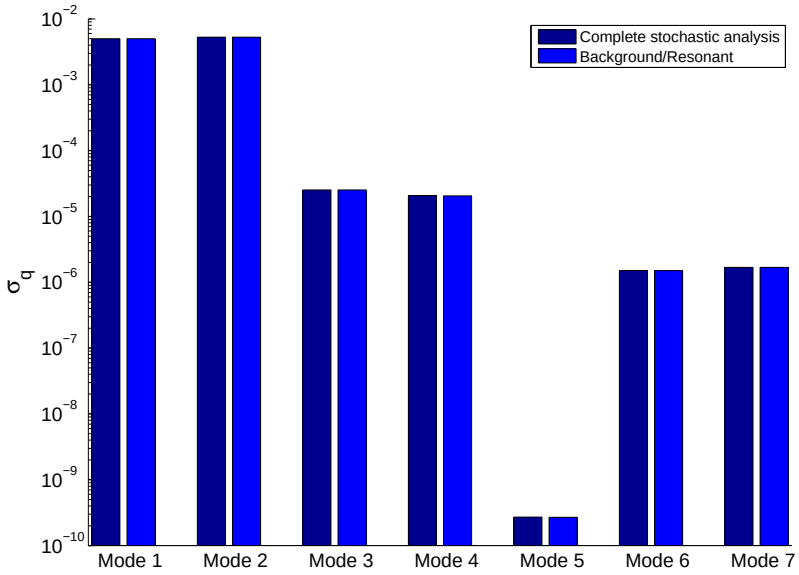

Figure B.12: Standard deviation of the modal displacement for the complete analysis and the B/R decomposition for an angle of attack of 45°.

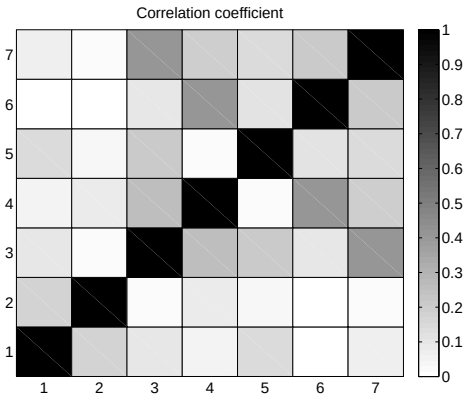

(a) Complete stochastic analysis.

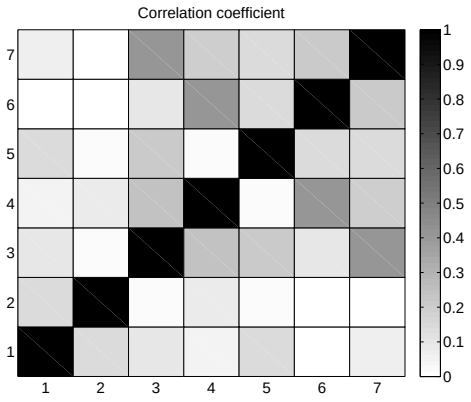

(b) Background/Resonant decomposition.

Figure B.13: Correlation coefficient of the modal displacement for an angle of attack of 15°.

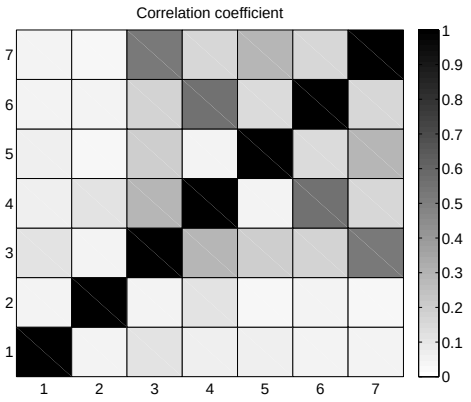

(a) Complete stochastic analysis.

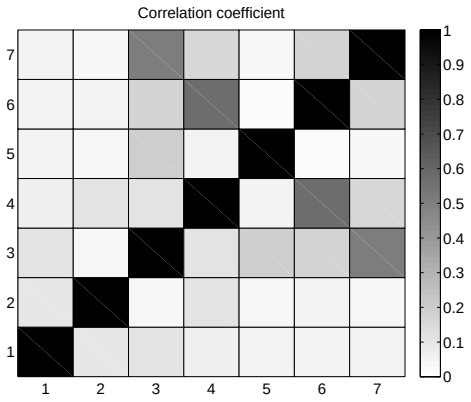

(b) Background/Resonant decomposition.

Figure B.14: Correlation coefficient of the modal displacement for an angle of attack of 45°.